

1 Tautomerism and Rotamerism of Favipiravir and Halogenated 2 Analogues in Solution and in the Solid State

3 Angel H. Romero,* Germán Fuentes, Leopoldo Suescun, Oscar Piro, Gustavo Echeverría,
4 Lourdes Gotopo, Horacio Pezaroglo, Guzmán Álvarez, Gustavo Cabrera, Hugo Cerecetto,
5 and Marcos Couto*



Cite This: <https://doi.org/10.1021/acs.joc.3c00777>



Read Online

ACCESS |



Metrics & More

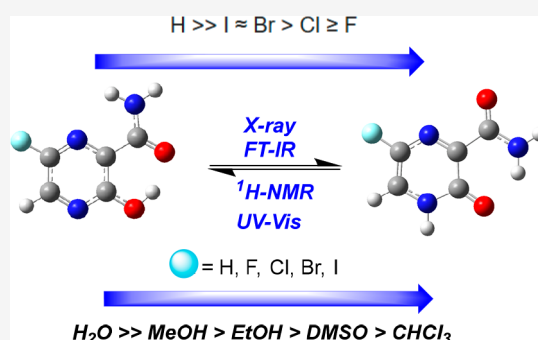


Article Recommendations



Supporting Information

6 **ABSTRACT:** Favipiravir is an important selective antiviral against RNA-
7 based viruses, and currently, it is being repurposed as a potential drug for the
8 treatment of COVID-19. This type of chemical system presents different
9 carboxamide-rotameric and hydroxyl-tautomeric states, which could be
10 essential for interpreting its selective antiviral activity. Herein, the tautomeric
11 3-hydroxypyrazine/3-pyrazinone pair of favipiravir and its 6-substituted
12 analogues, 6-Cl, 6-Br, 6-I, and 6-H, were fully investigated in solution and in
13 the solid state through ultraviolet–visible, ¹H nuclear magnetic resonance,
14 infrared spectroscopy, and X-ray diffraction techniques. Also, a study of the
15 gas phase was performed using density functional theory calculations. In
16 general, the keto–enol balance in these 3-hydroxy-2-pyrazinecarboxamides is
17 finely modulated by external and internal electrical variations via changes in
18 solvent polarity or by replacement of substituents at position 6. The enol tautomer was prevalent in an apolar environment, whereas
19 an increase in the level of the keto tautomer was favored by an increase in solvent polarity and, even moreso, with a strong hydrogen-
20 donor solvent. Keto tautomerization was favored either in solution or in the solid state with a decrease in 6-substituent
21 electronegativity as follows: H ≫ I ≈ Br > Cl ≥ F. Specific rotameric states based on carboxamide, “cisoide” and “transoide”, were
22 identified for the enol and keto tautomer, respectively; their rotamerism is dependent on the tautomerism and not the aggregation
23 state.

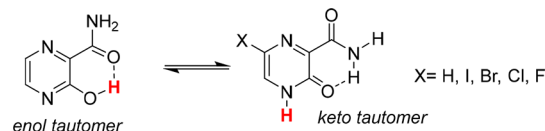


1. INTRODUCTION

24 Keto–enol tautomerism is one of the most important
25 equilibria in nature, being involved in a variety of chemical
26 and biological processes.^{1–6} It is operative in nucleic acid
27 bases, amino acids, and a great number of biochemical
28 processes that are dependent on proton-transfer reactions. For
29 example, it is supposed that the high level of histidine in active
30 sites of diverse types of enzymes may be associated with the
31 tautomerism of the NH proton into the imidazole ring, which
32 favors proton transfer in catalytic steps.^{7,8} Also, the canonical
33 keto-amino forms of DNA nucleobases play a pivotal role in
34 the formation of Watson–Crick base pairing structure via
35 intermolecular hydrogen bonding.^{9–11} The latter also plays an
36 important role in the design of anticancer and antiviral
37 chemotherapeutic agents based upon the lethal mutagenesis
38 concept; regardless of whether a sufficient number of
39 mutagenic nucleoside analogues are incorporated into viral
40 genomes, an increase in the rate of viral mutation occurs with
41 an affinity for viral replication.^{12–21} Meanwhile, rotamerism,
42 which is a concept that is less common than tautomerism, is
43 known to play an important role in the stabilization of peptide
44 and protein structures.^{22,23}

Favipiravir [1, T705 (X = F in Chart 1)] is a 3-hydroxy-2-
pyrazinecarboxamide with a fluorine atom at position 6. Its

Chart 1. Keto–Enol Tautomeric Equilibrium in 3-Hydroxy-2-pyrazinecarboxamide



structure is defined by the tautomeric 3-hydroxypyrazine/3-
pyrazinone (3HP/3OP) pair, where a hydrogen atom is
transferred between the N and O sites of the pyrazine ring, as
depicted in Chart 1. Also, favipiravir shows rotamerism
from the free rotation of the 2-carboxamide group. Favipiravir

Received: April 9, 2023



ACS Publications

© XXXX American Chemical Society

A

<https://doi.org/10.1021/acs.joc.3c00777>
J. Org. Chem. XXXX, XXX, XXX–XXX

has shown to be a potent antiviral against a broad spectrum of RNA viruses such as influenza viruses (types A–C),²⁴ H5N1 virus,²⁵ hepatotropic phlebovirus,²⁶ West Nile virus,²⁷ Norwalk virus (norovirus),²⁸ encephalitis viruses,²⁹ arenaviruses,³⁰ bunyavirus,³¹ and Ebola virus.³² Since the origin of the SARS-CoV-2 pandemic 2019 and in the absence of vaccines in the first year of the pandemic, this drug emerged as an attractive chemotherapeutic alternative, being extensively investigated in clinical trials and applied as medication in Russia, China, and India.^{33–35} Favipiravir was approved in India for COVID-19 treatment,³⁶ and in general, the drug has demonstrated to be effective for patients with moderate symptoms of COVID-19.³⁷ Currently, favipiravir is being repurposed for the treatment of COVID-19.^{38–40}

With regard to the origin of the antiviral activity of favipiravir, it is suggested as a guanine/adenine analogue that the (3HP/3OP) tautomerism and carboxamide rotamerism are pivotal issues in its selective antiviral activity. Favipiravir acts as a prodrug where its corresponding active T705-ribonucleotide is responsible for the blocking of the RNA replication in RNA viruses via selective inhibition of the RNA polymerase.⁴¹ That prodrug metabolite is formed through a nucleophilic substitution between the tautomeric NH nitrogen of favipiravir and the anomeric carbon of the furanose heterocycle, which could be favored by the presence of the keto tautomer. A recent study showed that 3-hydroxy-2-pyrazinecarboxamide (T-1105), the 6-hydrogenated analogue of favipiravir, displayed antiviral activities against influenza virus and foot-and-mouth disease virus on a scale comparable to that of favipiravir, but interestingly, treatment with T-1105 generated a significant proportion of the T-1105-ribonucleotide metabolite, which was larger than the proportions generated from T-705.⁴² The latter implies that T-1105 is more reactive than T-705, which could be attributed to the tentative dominance of the keto tautomer in 6-hydrogenated T-1105. On the contrary, molecular dynamics studies of favipiravir and its halogenated derivatives (6-Cl and 6-Br) on the RNA polymerase enzyme showed that the relative affinities of the keto tautomer of all halogenated derivatives for the RNA polymerase active site are barely higher than those found for the corresponding enol tautomers.⁴³ The effect of the halogen also was important, indicating that the enzyme affinities increase as a function of the halogen at position 6 in the following order: 6-Br ~ 6-Cl > 6-F. Then, understanding the keto–enol equilibrium in the 6-hydrogenated and -halogenated 3-hydroxy-2-pyrazinecarboxamides can be of great importance for directing the rational design of antiviral drugs, including those for treatment of COVID-19, based on the role of tautomerism/rotamerism as well as for interpreting the biological activity of some of their derivatives (e.g., favipiravir, 3-hydroxy-2-pyrazinecarboxamide, or a 6-brominated analogue).⁴²

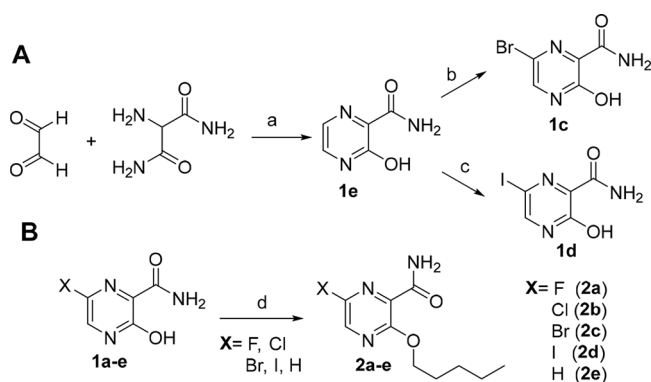
At the moment, there is scarce information relative to the tautomerism and rotamerism of favipiravir and its 6-substituted analogues. Recently, Antonov studied the tautomerism of favipiravir in solution (acetonitrile, toluene, and water) from theoretical and experimental points of view, finding that keto tautomerization is favored in a protic environment like water whereas the enol tautomerism is preferred in an aprotic solvent like acetonitrile and toluene.^{44a} Also, Antonov studied theoretically the tautomerism of the 6-hydrogenated analogue [X = H (Chart 1)] using the M06-2X/def2TZVP approach in solution and in the gas phase, finding that this 3-hydroxy-2-pyrazinecarboxamide has a stronger tendency toward keto

tautomerism than does favipiravir.^{44b} Meanwhile, Safin and Srimongkolpithak separately reported the crystal structure of favipiravir, showing the dominance of the enol tautomer in the solid state.^{44c,d} Other theoretical studies have provided information about the tautomerism of favipiravir and its 6-substituted analogues, finding that the keto tautomer may be favored in protic and polar environments.^{44e,f} Beyond the 3-hydroxy-2-pyrazinecarboxamides, other hydroxypyrazines tend to favor the keto tautomer in a protic solvent,⁴⁵ although the tautomeric equilibrium is slightly shifted toward the enol form in moderately polar and nonpolar environments.⁴⁶ It was also found that enol tautomerization in the hydroxypyrazines can be modulated by the incorporation of an electron-deficient substituent into the pyrazine ring. For example, from ultraviolet (UV) spectroscopy studies, the 2,6-dihydroxy-3,5-diphenylpyrazine was found as 6-hydroxy-3,5-diphenylpyrazine-2-one (keto tautomer) in a protic solution, whereas its 6-chlorinated analogue, 2-chloro-6-hydroxy-3,5-diphenylpyrazine, was prevalently found as the enol tautomer.^{45b} Despite the advances in the study of favipiravir, a more detailed study of favipiravir and its 6-substituted analogues is needed to provide a general vision of the factors governing tautomerism and rotamerism in this type of 3-hydroxy-2-pyrazinecarboxamide. It could be useful for the rational design of antivirals and for interpreting the selective antivirals of these analogues. Herein, we investigate the tautomerism and rotamerism of favipiravir and its 6-hydrogenated and -halogenated 3-hydroxy-2-pyrazinecarboxamides either in the solid state or in solution through ultraviolet–visible (UV–vis)/nuclear magnetic resonance (NMR) spectroscopic studies and X-ray crystallography/Fourier transform infrared (FTIR) spectroscopic analysis, respectively. The main goal is to understand how the internal and external electronic influence may modulate the tautomeric and rotameric states of the 6-substituted 3-hydroxy-2-pyrazinecarboxamides, seeking to understand how keto tautomerization may be favored. The internal influence was studied by the incorporation of different groups with a varied electronic nature (F, Cl, Br, I, and H) at position 6 of the pyrazine ring, whereas the external influence was studied by changes in the polarity of the solvent. To complement, a conformational theoretical study in the gas phase was performed to interpret the relative thermodynamic stability of tautomers and to understand the factors that govern the tautomeric equilibrium.

2. RESULTS AND DISCUSSION

2.1. Chemical Synthesis. This tautomeric and rotameric study was focused on five 3-hydroxy-2-pyrazinecarboxamides functionalized at position 6 with halogens (F, Cl, Br, and I) and a hydrogen atom (H). The corresponding fluorine (**1a**) and chlorine (**1b**) derivatives were purchased from commercial sources, whereas the rest of the 3-hydroxy-2-pyrazinecarboxamides (**1c–e**) were prepared from reported strategies with a few modifications as depicted in Scheme 1A. Compound **1e** was prepared by condensing the 2-aminomalonodiamide with glyoxal (60%).⁴⁷ Meanwhile, **1c** and **1d** were prepared by halogenation of **1e** with NBS⁴⁸ and NIS,⁴⁹ respectively, in DMF upon controlled heating (80 °C). With 3-hydroxy-2-pyrazinecarboxamides **1a–e** in hand, their O-alkylated forms (**2a–e**, respectively) were synthesized by coupling the corresponding 3-hydroxy-2-pyrazinecarboxamides (**1a–e**) with an excess of *n*-pentyl iodide under heating (Scheme 1B).⁵⁰ Compounds **2a–e** were prepared for the purpose of

Scheme 1. Synthetic Strategies for the Preparation of (A) 3-Hydroxy-2-pyrazinecarboxamides 1a–c and (B) Their O-Alkylated Analogues 2a–e^a



^aReaction conditions: (a) H₃PO₄ (20%), concentrated HCl, 80 °C, 2 h; (b) NBS (1.6 equiv), DMF, 80 °C, 6 h; (c) NIS (1.6 equiv), DMF, 80 °C, 6 h; (d) *n*-pentyl iodide (5–10 equiv), 100 °C, 12 h.

the electronic nature of the 6-substitution, revealing a consistent decrease in the magnitude of the calculated energy difference for the keto–enol equilibrium (more negative) in the following order as a function of 6-functionalization: 6-F > 6-Cl > 6-Br > 6-I > 6-H. Interestingly, it was found that each tautomeric form presented a specific rotameric carboxamide configuration. The enol tautomer was characterized by having a “cisoide” rotameric carboxamide moiety with respect to the 3-hydroxyl moiety, which implies the 3-oxo/hydroxyl moiety in front of the 2-carboxamide oxygen that is stabilized by an intramolecular hydrogen bond between the hydroxyl hydrogen and the carboxamide oxygen (–O–H–O=C–NH₂–), as depicted in Table 1. Meanwhile the keto tautomer showed a “transoide” conformation for the 2-carboxamide moiety, where the 3-oxo/hydroxyl moiety is in an opposite orientation to the 2-carboxamide oxygen and the rotameric stage is stabilized by an intramolecular hydrogen bond between the 3-oxopyrazine moiety and one of the carboxamide NH₂ protons (–C=O–H–NH–CO–), as depicted in Table 1. On the contrary, a similar tendency was found via the B3LYP/6-31G(d,p) approach with a small deviation in the tendency for the 6-iodo derivative, 1e (Table 1).

To obtain more information about the carboxamide rotamerism, a conformational analysis was performed on 6-fluoro-3-hydroxy-2-pyrazinecarboxamide 1a as the platform model. The conformational analysis for the enol tautomer was focused on structures having a rotating hydroxyl moiety with a “cisoide” (Figure 1A) or “transoide” carboxamide, whereas the keto tautomer was focused on structures having only a rotating carboxamide moiety (Figure 1C).^{55–58} Within the enol tautomer, there are four preferential conformational forms: E_A, E_B, E_C, and E_D (Figure 1D). Among them, enol tautomer E_A (“cisoide” carboxamide) was identified as the most stable enolic conformer, followed by conformer E_C (“transoide” carboxamide) (ΔE = 2.0 kcal/mol) and least stable conformers E_B (ΔE = 5.9 kcal/mol) and E_D (ΔE = 5.9 kcal/mol). Among the “cisoide” rotameric states (E_A and E_B) of the enol tautomer, it should be noted that the existence of an intramolecular hydrogen bond between the carboxamide oxygen and the hydroxylic hydrogen (–O–H–O=C–NH₂–) stabilized the enol tautomer in E_A. Meanwhile, among the “transoide” rotameric states of the enol tautomer, the stabilization via hydrogen bonding between one

Table 1. Relative Stabilities of the Most Stable Enol and Keto Tautomers of 3-Hydroxy-2-pyrazinecarboxamides 1a–e in the Gas Phase

entry	compound (X)	<i>E</i> _{tot} (kcal/mol) ^a		Δ <i>E</i> _{keto–enol} ^b (kcal/mol)	Δ <i>E</i> _{keto–enol} ^c (kcal/mol)
		enol	keto		
1	1a (F)	–381226.8	–381213.4	–13.37	–12.60
2	1b (Cl)	–607344.4	–607331.8	–12.63	–11.94
3	1c (Br)	–1933875.0	–1933862.4	–12.54	–11.74
4	1d (I)	–505330.2	–505318.0	–12.16	–12.03
5	1e (H)	–318943.7	–318933.4	–10.26	–9.62

^aCalculations derived from M06-2X/def2TZVP. ^bEnergy differences derived from M06-2X/def2TZVP. ^cEnergy differences derived from B3LYP/6-31G(d,p). Individual total energies for enol and keto tautomers for 1a–e can be found in Table ST2.

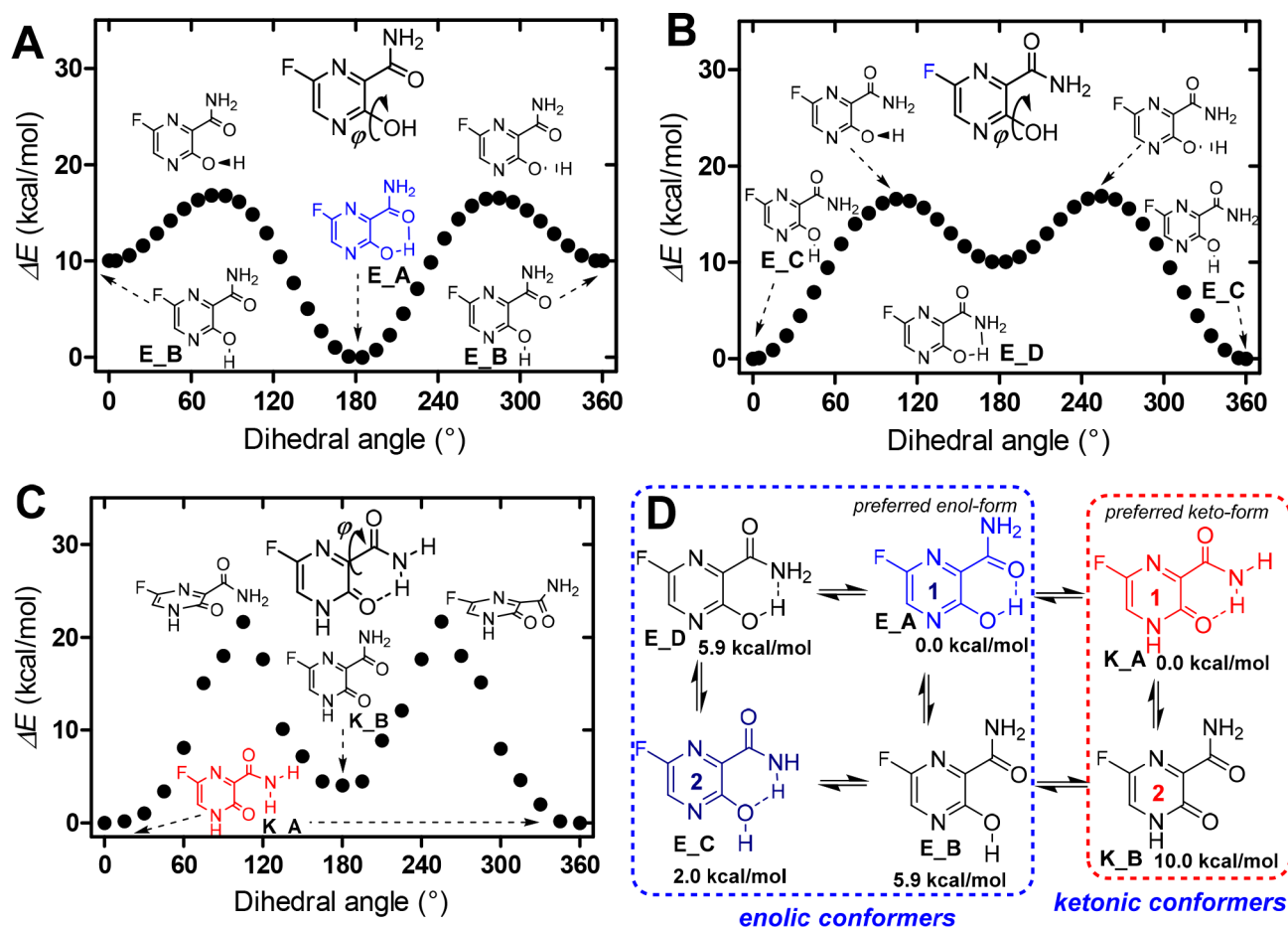


Figure 1. Conformational analysis of (A and B) enol and (C) keto tautomers of favipiravir relative to the dihedral angle between the pyrazine ring plane and the rotating carboxamide/hydroxyl moieties. (D) General scheme of the most stable enol and keto tautomers of favipiravir. Note that the energies of the enol tautomers (E_B, E_C, and E_D) and the keto tautomer (K_B) are indicated as a function of the most stable enol tautomer (E_A) and keto tautomer (K_A), respectively, as differences in energies. Conformational energies were determined via the M06-2X/def2TZVP approach.

241 of the carboxamide NH_2 protons and the hydroxylic oxygen
 242 ($\text{O}=\text{C}-\text{NH}-\text{H}-\text{O}-\text{H}$) in conformer E_C is more favorable
 243 than that established between the carboxamide nitrogen and
 244 hydroxylic proton [$\text{O}=\text{C}(\text{H}_2\text{N})-\text{H}-\text{O}-$] in conformer E-D.
 245 With regard to the keto tautomer, the computed energies of
 246 the different conformers confirmed that the K_A tautomer was
 247 clearly the most preferred conformer, whereas the K_B
 248 tautomer was recognized as the second most stable conformer
 249 with an energy difference of 10.0 kcal/mol (Figure 1D).
 250 Tautomer K_A was characterized by a “transoid” conforma-
 251 tion featuring intramolecular hydrogen bonding between one
 252 of the carboxamide NH_2 protons and the 3-oxo moiety.
 253 Conformers of the keto tautomers having the 2-carboxamide
 254 oriented out of the molecular pyrazine plane were identified as
 255 the most energetic conformers (less stable) by >18.8 kcal/mol
 256 (Figure 1C). Like the ketonic conformers, enolic conformers
 257 having hydroxyl or carboxamide groups out of the molecular
 258 plane displayed the highest total energies (6.3–12.6 kcal/mol
 259 over tautomer K_A) (Figure 1A,B). All of these tendencies
 260 found for the enol or keto tautomers of favipiravir are expected
 261 to be similar for the rest of the studied 3-hydroxy-2-
 262 pyrazinecarboxamides 1b–e and could be the dominant
 263 tendency in solution and in the solid state.

264 **2.3. Tautomerism and Rotamerism in the Solid State.**
 265 To gain insight into the tautomeric and rotameric forms of the

3-hydroxy-2-pyrazinecarboxamides 1a–e in the solid state, X-
 ray crystallographic and infrared spectroscopic analyses were
 performed. Beginning with the X-ray diffraction analysis, the
 crystal structures of all studied 3-hydroxy-2-pyrazinecarbox-
 amides 1a–e and some of their 3-O-alkylated analogues (2b–
 d) were determined. ORTEP structures are shown in Figures
 2A–E and 3A–C for compounds 1a–e and 2b–d,
 respectively. From 3-hydroxy-2-pyrazinecarboxamides 1a–e,
 their crystal structure allowed us to identify the dominant
 tautomer in the solid state, which provided us a general
 perspective of keto–enol tautomerism for each of the 3-
 hydroxy-2-pyrazinecarboxamides 1a–e. For compounds 1a
 and 1b, only the enol tautomer was distinguished from their
 crystalline structures (panels A and B, respectively, of Figure
 2). That enol tautomer showed a “cisoide” conformation for
 the 2-carboxamide moiety with the formation of an
 intermolecular hydrogen bond between the 3-hydroxylic
 proton and the carboxamide oxygen ($3-\text{O}-\text{H}-\text{O}=\text{C}-\text{NH}_2$).
 This H-bond was also described in the gas phase studies for
 the enol tautomer (Figure 1A). Meanwhile, a keto/enol
 mixture was found for the 6-bromo (1c) and 6-iodo (1d) 3-
 hydroxy-2-pyrazinecarboxamides with a keto–enol distribution
 in the solid state of 1:2 for the 6-bromo molecule and 2:1 for
 the 6-iodo molecule (Figure 3A,B). Importantly, their keto
 tautomers exhibited a common rotameric state with a 290

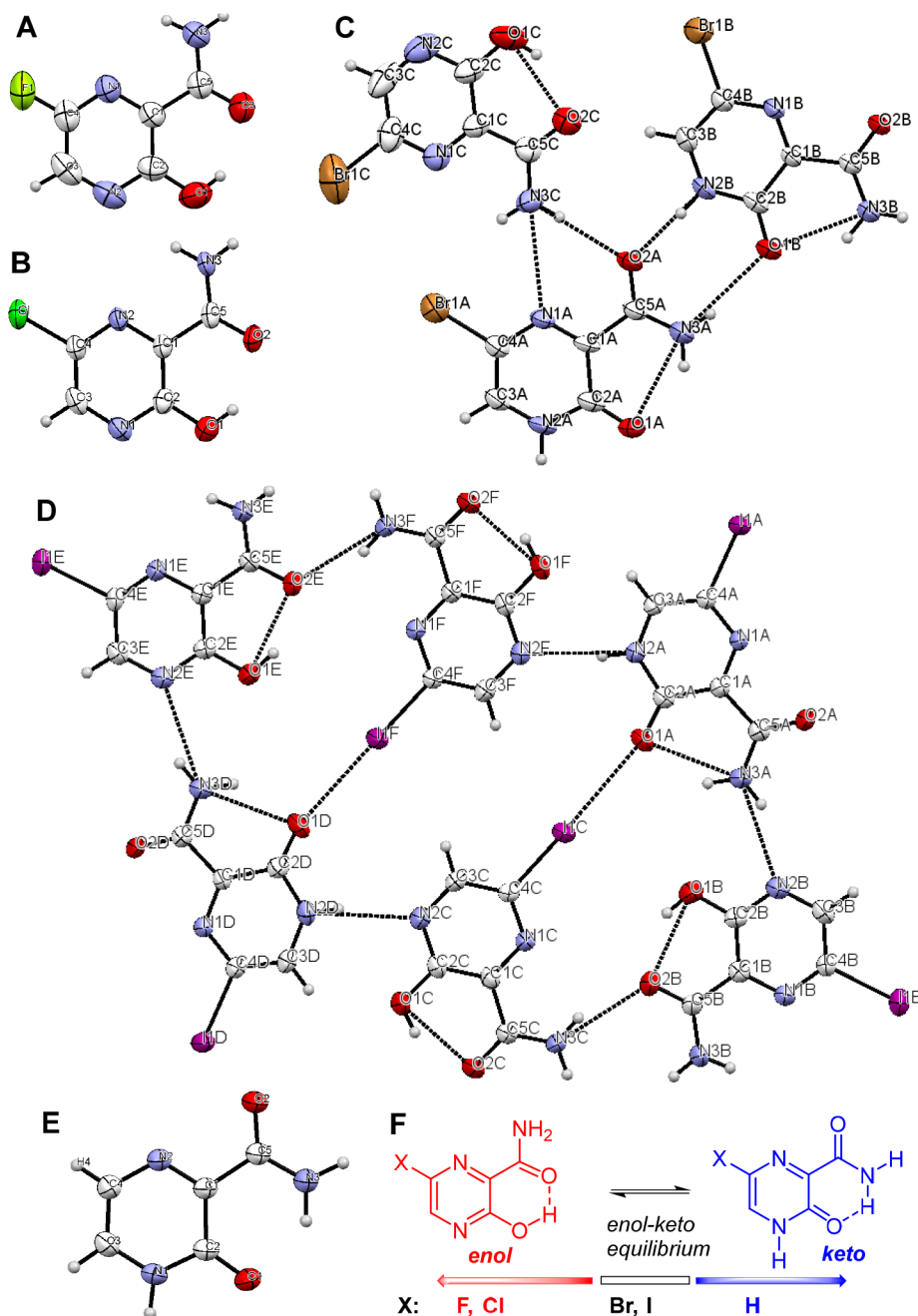


Figure 2. Tautomers and rotamers identified in the solid state for the studied 3-hydroxy-2-pyrazinecarboxamides (A) 1a, (B) 1b, (C) 1c, (D) 1d, and (E) 1e: white for carbon, blue for nitrogen, gray for hydrogen, light green for fluorine, green for chlorine, light brown for bromine, and purple for iodine. (F) General dependence of tautomerism as a function of the 6-substitution. ORTEP drawings of compounds 1a–e showing thermal ellipsoids at the 50% probability level.

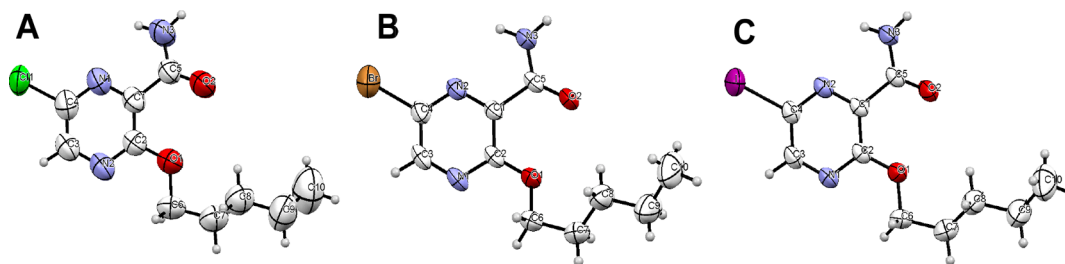
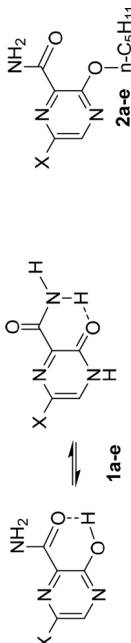


Figure 3. Crystal structures of 3-O-alkylated analogues (A) 2b, (B) 2c, and (C) 2d. ORTEP drawings of compounds 2b–d showing thermal ellipsoids at the 50% probability level.

Table 2. Infrared Bands [in cm^{-1} (intensities in parentheses)] for Tautomeric 3-Hydroxy-2-pyrazinecarboxamides 1a–e and Their 3-O-Alkylated Analogues 2a–e


	vibrational band	2a	1a	2b	1b	2c	1c	2d	1d	2e	1e
1	N–H ν_s	3390 (19)	3349 (10)	3464 (15)	3343 (16)	3462 (20)	3426 (14)	3462 (18)	3432 (8)	3360 (18)	3352 (12)
	N–H ν_{as}	3364 (19)								3302 (10)	broad
2	N–H ν_g	3224 (11)	3214 (17)	3260 (6)	3271 (13)	3275 (11)	3273 (12)	~3200 (18)	3223 (8)	3182 (14)	~3150 (8)
	N–H ν_{as} or O–H ν_s	~3190 (10)		~3150 (8)	3206 (19)	~3200 (15)	3225 (14)	~3150 (10)		3131 (12)	~3100 (8)
3	C–H ν_s	2955 (21)	2972 (12)	~3100 (10)	2931 (12)	3138 (17)	3142 (12)	2949 (20)	2982 (7)	2957 (18)	2980 (16)
	C–H ν_{as}	2931 (12)	2853 (8)	2951 (12)	2889 (11)	2951 (19)	2951 (11)	2920 (19)		2891 (10)	2937 (14)
		2850 (9)		2850 (8)		2895 (17)	2855 (10)	2852 (14)			
4	C=O ν_s	1679 (63)	1670 (37)	1705 (25)	1669 (47)	1703 (34)	1682 (22)	1703 (33)	1674 (12)	1659 (45)	1684 (23)
	C=O $\nu_{(ii)}$ ν_s	1613 (21)	1653 (33)			1645 (18)	1645 (25)	1668 (28)	1636 (14)	1645 (45)	1650 (25)
5	C=N ν_s	1613 (21)	1600 (22)	1589 (13)	1604 (30)	1589 (20)	1593 (23)	1587 (17)	1593 (12)	1622 (45)	1585 (22)
	C=C ν_s	1559 (25)	1558 (20)	1540 (8)	1532 (18)	1546 (15)	1558 (23)	1539 (14)	1558 (16)	1568 (21)	1541 (20)
	C=C ν_{as}			1518 (8)		1525 (16)		1519 (13)		1533 (25)	
6	N–H δ	1430 (64)	1465 (19)	1470 (16)	1470 (48)	1470 (26)	1460 (37)	1467 (19)	1429 (22)	1465 (18)	1445 (17)
			1430 (50)	1433 (25)				1429 (27)		1435 (44)	

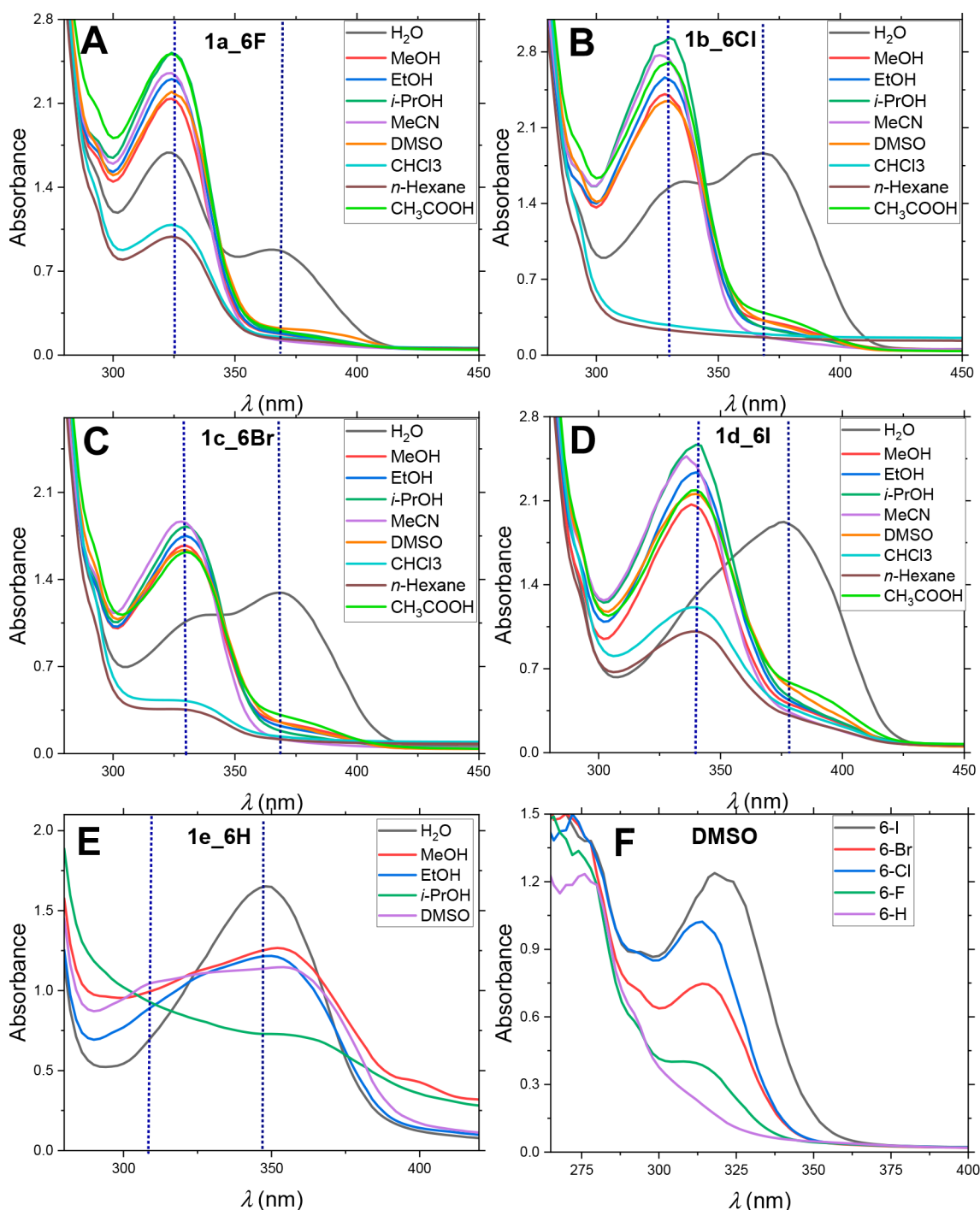
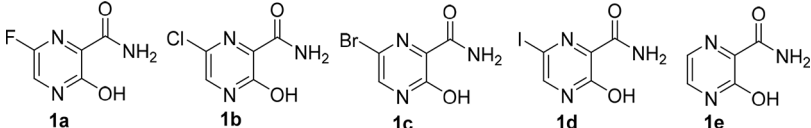


Figure 4. UV-vis spectra of 3-hydroxy-2-pyrazinecarboxamides **1a–e** in different environments (A–E, respectively) and O-pentyl derivatives under DMSO (F). Further UV-vis spectra for O-pentyl derivatives in different solvents can be found in Figure S14.

291 “transoid” 2-carboxamide conformation showing an intra-
 292 molecular hydrogen bond between one of the carboxamide
 293 NH₂ protons and the 3-oxo oxygen (–CONH–H–O=C–),
 294 whereas their enol tautomers showed a “cisoide” rotameric
 295 conformation. With regard to 6-bromo derivative **1c**, the three
 296 symmetry-independent tautomers were connected through five
 297 intermolecular hydrogen bonds. (i) Two of these hydrogen
 298 interactions connect two keto tautomers through the NH
 299 pyrazine proton and the 3-oxo moiety of one of them with the
 300 carboxamide oxygen and carboxamide NH₂ proton, respec-
 301 tively, of the other keto tautomer. (ii) The other two hydrogen

bonding interactions connect an enol tautomer through its 2-
 carboxamide NH₂ protons with the pyrazine N1 and
 carboxamide oxygen of one of the keto tautomers. (iii) The
 last intermolecular bonding connects an enol tautomer through
 its carboxamide oxygen with the C–H aromatic proton of one
 of the keto tautomers as depicted in Figure 2C. Meanwhile, the
 crystal structure of compound **1d** was determined to be a
 cyclic hexamer (two keto tautomers vs four enol tautomers),
 which was stabilized by eight intermolecular hydrogen bonding
 interactions. Each keto tautomer interacts simultaneously with
 three enol tautomers, forming two hydrogen bonds through its

Table 3. UV–Vis Absorption Bands for 3-Hydroxy-2-pyrazinecarboxamides **1a–e** in Different Solvents


	λ_{abs} (nm) (enol:keto ratio) ^a								
	gas phase ^b	H ₂ O	MeOH	EtOH	<i>i</i> -PrOH	MeCN	DMSO	<i>n</i> -hexane	acetic acid
1a	280.0/320.4	322/366 (1.9)	324/370 (12.4)	324/370 (13.1)	324/370 (13.0)	324/370 (19.6)	324/372 (10.1)	324	324
1b	282.0/321.6	336/368 (0.83)	328/368 (7.5)	328/370 (10.2)	330/370 (11.8)	326/370 (16.8)	330/372 (8.7)	328	330
1c	308.6/341.1	340/370 (0.77)	330/372 (5.0)	330/372 (8.4)	330/372 (11.0)	328/370 (17.4)	330/370 (7.1)	328	330
1d	304.6/347.1	344/376 (0.71)	338/372 (4.3)	340/376 (5.1)	340/376 (5.1)	338/378 (7.3)	340/380 (4.1)	340	340
1e	270.4/297.8	310/348 (0.0)	312/346 (1.2)	— ^c	— ^c	302/348 (4.8)	308/356 (1.9)	— ^c	344

^aThe enol:keto ratio was estimated from a mean between the total areas of the absorption enol (lower band) and keto (higher band) wavelengths as follows: $A_{\text{enol}}/A_{\text{keto}}$. ^bTheoretical absorption wavelengths calculated in the gas phase [B3LYP/6-31G(d,p)]. ^cNo measurement by low solubility.

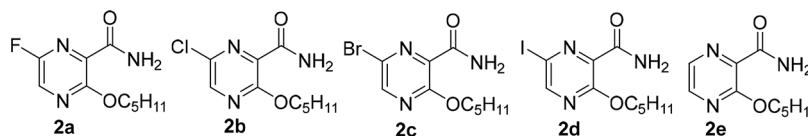
pyrazine NH proton and one of their carboxamide NH₂ protons with pyrazine N4 of two enol tautomers, and the interaction with the third enol tautomer is a halogen bond between its iodine atom as the σ -hole and the carboxamide oxygen of the enol tautomer as the electron donor. This implies six intermolecular interactions. The other two interactions were derived from two pairs of enol tautomers, where each pair consisted of hydrogen bonds between one of the carboxamide NH₂ protons of one of the enol tautomers and the carboxamide oxygen of the other enol tautomer. With regard to 3-hydroxy-2-pyrazinecarboxamide **1e**, its crystal structure is constituted purely by the keto tautomer. That keto tautomer showed a specific “transoid” carboxamide conformation as described above. Further X-ray details such as the packing rearrangement, intermolecular interactions, and general crystallographic data can be found in Figures S1–S5 and Tables S1–S51.

To gain further insight into the rotamerism of this type of structure, we analyzed the rotamerism in the solid state of some of their 3-O-alkylated analogues (**2b–d**), which is the closest version of the enol tautomer of compounds **1a–e**. From the X-ray data, all three 3-O-alkylated analogues showed a “cisoide” rotameric carboxamide (Figure 3A–C). That rotameric disposition is similar to that found for the enol tautomer of compounds **1a–e**, which reflects the fact that the carboxamide rotamerism in this type of chemical structure is a chemical property more dependent on the tautomerism than on internal electronic changes in the pyrazine ring. Further crystallographic information and the typical crystal packing rearrangement can be found in Figures S6–S8.

To complement the analysis in the solid state, the vibrational bands of 3-hydroxy-2-pyrazinecarboxamides **1a–e** and their O-alkylated analogues **2a–e** were analyzed from IR spectra. IR spectra and a summary of the data can be found in Figures S9–S13 and Table 2, respectively. The IR spectra of compounds **2a–e** allowed us to obtain an approximation of the typical vibrational bands of the enol tautomers of compounds **1a–e**. In general, from 3-O-alkylated analogues, it should be noted that compounds **2a** and **2b** showed similar vibrational bands (in magnitude and relative intensity) compared to those of their hydroxyl analogues **1a** and **1b**, respectively, which supports the idea that these 3-hydroxy-2-pyrazinecarboxamides are predominantly enolic tautomers in the solid state (see entries 4 and 5 of Table 2). In addition, a higher intensity for the IR band in the 3200 cm^{−1} region in compounds **1a** and **1b** compared to that region of their 3-O-alkylated analogues also

supports the existence of the enol tautomer because the stretching vibration of the H–O bond increases the relative intensity of the IR band at 3200 cm^{−1}. Meanwhile, for compounds **1c–e**, appreciable differences compared to their O-alkylated analogues were observed for the 1700–1620 cm^{−1} (C=O stretching) or 1600–1500 cm^{−1} (C=N and C=C stretching) region. In these IR regions, 3-O-alkylated analogues **2c–e** were characterized by a unique IR band at 1700 cm^{−1} concerning the typical C=O stretching as well as a pair of IR bands at 1590–1570 and 1560–1530 cm^{−1} with a relatively higher abundance from 1.3- to 1.8-fold for the first one. In contrast, for compounds **1c–e**, the following observations were made: (i) a new IR band in the 1700–1620 cm^{−1} zone having two IR bands at 1680 and 1640 cm^{−1} of comparable abundances and (ii) a comparable abundance between their two IR bands at 1600–1500 cm^{−1}, the IR band at 1560–1530 cm^{−1} being barely more abundant than the IR band at 1590–1560 cm^{−1} in some cases. Another important difference found for compounds **1c–e** in contrast to their 3-O-alkylated analogues was a significant reduction of the 3220 cm^{−1} band. All of these mentioned features supported the idea that compounds **1c–e** are mainly in their keto tautomeric forms or exist as an enol/keto mixture with the keto tautomer being slightly dominant in one case, i.e., compound **1e**. Finally, a comparison among compounds **1a–e** in the IR region near 3400 cm^{−1} and near 3200 cm^{−1} showed that the intensity of the IR band at 3200 cm^{−1} was higher than that of the IR band at 3340–3460 cm^{−1} for compounds **1a** and **1b**, while a more equivalent proportion between the mentioned IR bands was found for compounds **1c** and **1d**. Meanwhile, compound **1e** displayed an IR band at 3352 cm^{−1} with an intensity that was higher than that of the almost unappreciable IR band at 3150 cm^{−1}. All of this evidence, assuming that the IR band at 3200 cm^{−1} corresponds in part to the stretching of the H–O bond, supports the idea that compounds **1a** and **1b** are found preferentially in the enol form, compounds **1c** and **1d** are found as a clear enol/keto mixture, and compound **1e** is found predominantly or purely in the keto form.

2.4. Tautomeric Structures in Solution. The tautomeric equilibrium of 3-hydroxy-2-pyrazinecarboxamides **1a–e** was initially investigated through UV–vis spectroscopy using various solvents. From UV–vis spectra, two absorption bands were distinguished from a fresh solution of 3-hydroxy-2-pyrazinecarboxamides **1a–e** (Figure 4). In general, halogenated pyrazines **1a–d** exhibited two absorption bands at 322–340 and 370–376 nm, whereas nonhalogenated pyrazine

Table 4. UV–Vis Absorption Bands for 3-O-Pentyl-2-pyrazinecarboxamides **2a–e** in Different Solvents

entry	compound	λ_{abs} (nm)			
		H ₂ O	MeOH	MeCN	DMSO
1	2a	316	312	310	308
2	2b	322	316	316	314
3	2c	322	318	316	314
4	2d	330	322	318	318
5	2e	278	278	276	274

1e displayed minor absorption bands at 300–312 and 346–356 nm (Table 3). In an effort to associate each absorption band to each tautomeric form (enol or keto tautomer) of the 3-hydroxy-2-pyrazinecarboxamides, first, we analyzed the UV spectra of their 3-O-alkylated derivatives **2a–e** to obtain an approximation of the absorption band of the enol forms of **1a–e** (Table 4). From the UV–vis spectra of 3-O-alkylated analogues **2a–e**, a unique absorption band was found for all O-alkylated derivatives **2a–e** with absorption values from 308 to 330 nm for halogenated compounds **2a–d** and from 274 to 278 nm for nonhalogenated derivative **2e**. These absorption bands are comparable in magnitude to the lowest absorption bands found for compounds **1a–e**, which suggests that the typical lowest absorption found for 3-hydroxy-2-pyrazinecarboxamides **1a–e** is associated with the enol tautomer, whereas the largest values can be attributed to the keto tautomer. To support the assignment further, a theoretical absorption study using the B3LYP/6-31G(d,p) approach was performed in the gas phase for the keto and enol forms of derivatives **1a–e**. From the optimized structures, the enol tautomers presented the lowest absorption bands with values ranging from 279 to 309 nm, whereas the keto tautomers displayed the largest absorption bands from 320 to 347 nm (Table 3). According to these theoretical data, the lowest absorption values found from the experimental measurements correspond to the enol tautomer of the 3-hydroxy-2-pyrazinecarboxamides, whereas the highest absorption bands are associated with the keto tautomer. Additional calculations were performed using the M06-2X/def2TZVP functional, but that approach provided us with an underestimation of the absorption bands (Table ST2). With the correct matching between absorption wavelengths with each one of the tautomeric forms of the tested 3-hydroxy-2-pyrazinecarboxamides, it should be noted that the keto/enol balance of these hydroxyl-pyrazines depends on two factors: (i) the nature of the solvent and (ii) the substitution at position 6. Beginning with the effect of the solvent, in general, the enol tautomer was identified as the main tautomeric form for most of the studied pyrazines **1a–e**, although its prevalence in solution was more remarkable with a decrease in polarity and hydrogen-donor nature of the solvent as follows: *n*-hexane \sim CHCl₃ > MeCN > *i*-PrOH > DMSO > EtOH > MeOH > water (Table 3). An almost exclusive enol tautomer was detected in a nonpolar solvent like chloroform or *n*-hexane for most of studied compounds **1a–e**, a dominance of the enol tautomer over the keto tautomer in polar solvents like acetonitrile and DMSO with enol:keto ratios of 19.6–10.1, 16.8–8.7, 17.4–7.1, 7.3–4.1, and 4.8–1.9 for compounds **1a–e**, respectively, a remarkable enol/keto balance with discrete

dominance of the enol tautomer in protic solvents like alcohols with enol:keto ratios of approximately 12, 7–10, 5–8, 4–5, and 1.2 for compounds **1a–e**, respectively, and a prevalence of the keto tautomer in most of the cases (except compound **1a**) in a water solvent with enol:keto ratios of 1.9, 0.83, 0.77, 0.71, and 0 for compounds **1a–e**, respectively. Table 3 shows that it should be noted that the tautomeric balance is dependent on the chemical function at position 6, where the enol proportion increases with the electronegativity of that 6-function as follows: 6-F > 6-Cl > 6-Br > 6-I > 6-H. This indicates, for example, for compound **1e** (6-H) the strong dominance of the keto tautomer in water (almost 100% abundance), a comparable existence in methanol (~50%), and an appreciable occurrence in nonprotic solvents (Table 3). Then, the UV–vis technique offered a good perspective on the tautomerism of 3-hydroxy-2-pyrazinecarboxamides **1a–e**, although it did not provide useful information to elucidate the rotameric configuration of the carboxamide moiety.

To obtain information about carboxamide rotamerism in solution, a ¹H NMR study was performed using different deuterated solvents taking advantage of the possible chemical differences between the carboxamido NH₂ protons of the keto tautomeric form (see the keto tautomer in Figure 5). From ¹H NMR spectra, it should be noted that there is a significant difference between the chemical shifts of the carboxamide NH₂ protons as a function of solvent polarity (Table 5). That difference increased with the polarity and hydrogen-donor character of the solvent for all studied 3-hydroxy-2-pyrazinecarboxamides **1a–e**, being almost zero for a nonpolar solvent like chloroform. For example, for 6-fluorinated derivative **1a**, a chemical shift difference of 0.45 ppm was found in water, and a continuous decrease in the chemical shift difference was observed with a decrease in the polarity and hydrogen-donor nature of the solvent, i.e., 0.4, 0.33, 0.23, and 0.06 ppm for methanol, acetonitrile, DMSO, and chloroform, respectively. Halogenated derivatives **1b–d** displayed a similar shift difference trend with approximate values of 0.7, 0.48, 0.3, 0.26, and 0.07 ppm in water, methanol, acetonitrile, DMSO, and chloroform, respectively, whereas nonhalogenated derivative **1e** displayed higher shift differences under all environments with values of 1.04, 0.82, 0.65, 0.58, and 0.67 ppm in water, methanol, acetonitrile, DMSO, and chloroform, respectively. In general, the chemical shift difference between the carboxamido NH₂ protons increased with an increase in solvent polarity or a decrease in 6-substitution electronegativity, this behavior being similar to that observed for the tautomeric forms of 3-hydroxy-2-pyrazinecarboxamides **1a–e** in solution. Thus, it is clear that the rotamerism is a 500

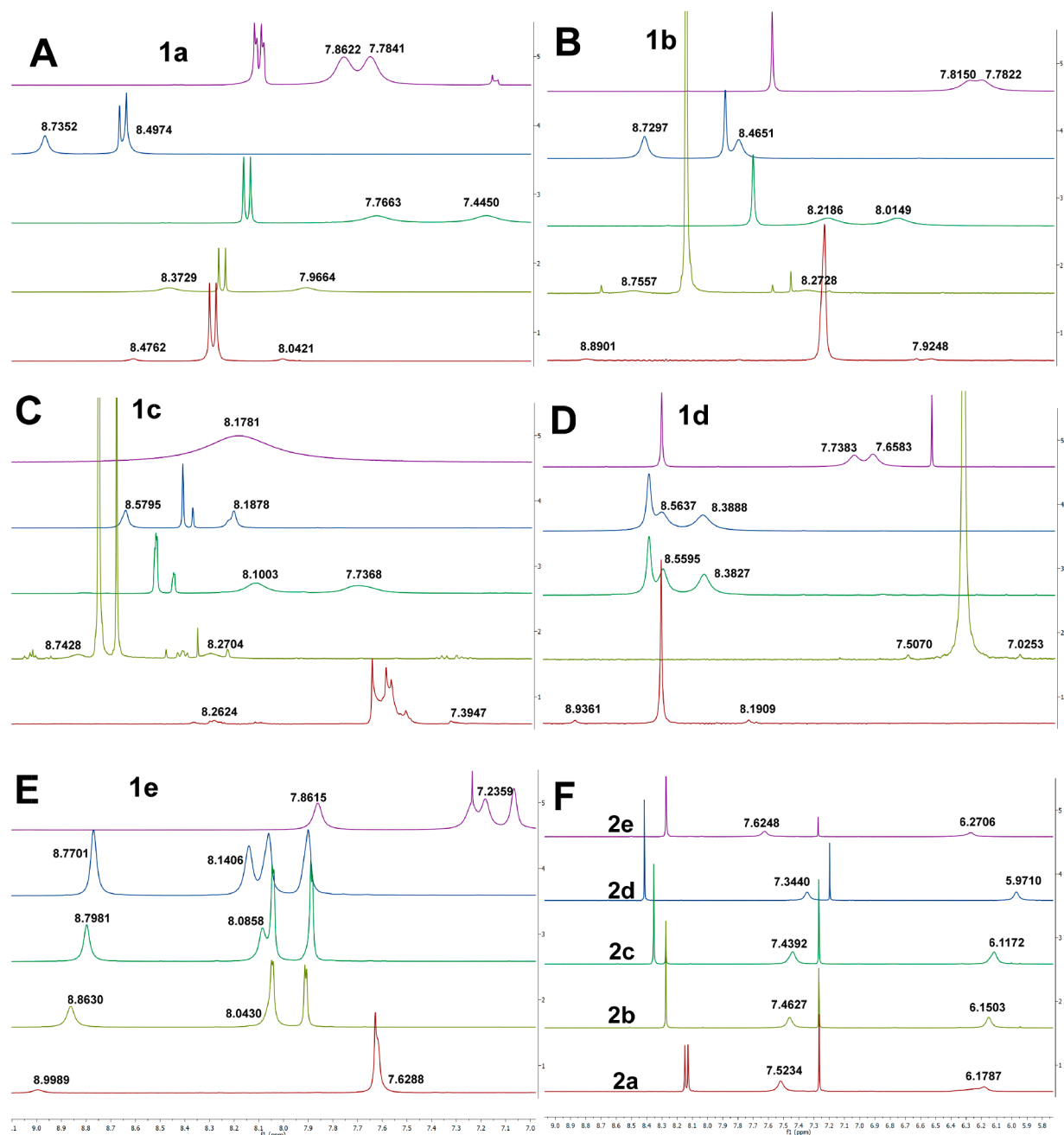


Figure 5. ^1H NMR spectra of 3-hydroxy-2-pyrazinecarboxamides **1a–e** under different environments (A–E, respectively) and the *O*-pentyl derivative in $\text{DMSO}-d_6$ (F). Chemical shifts expressed in parts per million, and spectra visualized in a window from 5.8 to 9.0 ppm. Further detailed spectra can be found in Figures S15–S19.

function of the tautomerism and, a “transoide” carboxamido moiety, which exhibits distinguished differences in the chemical shifts of its carboxamido protons, can be mainly found in protic environments that favor keto tautomerization. To establish a correlation between the enol:keto proportions and chemical shift differences between carboxamido NH_2 protons, we plotted the enol:keto proportions, derived from UV–vis spectra, against the chemical shift differences between the carboxamido NH_2 protons (Figure 6). In general, good correlations were found in different solvents (water, methanol, acetonitrile, and DMSO), where, consistently, the enol:keto ratios decreased with an increase in the chemical shift difference. That consistent and linear correlation confirmed that the keto tautomer is dominated by a “transoide” rotameric

conformation [K_A (Figure 1D)] in solution, whereas the enol tautomer is defined by having a “cisoide” rotameric conformation [E_A (Figure 1D)]. Thus, the large chemical shift difference between the carboxamide NH_2 protons under polar or protic environments implies that compounds **1a–e** are predominantly found as the keto tautomer, which is a tautomeric form characterized by two differentiated carboxamide protons derived from the “transoide” conformation. Meanwhile, the discrete or null chemical shift difference between the carboxamide protons in a nonpolar environment reveals that compounds **1a–e** are prevalently found in the enol form, whose carboxamide NH_2 protons are differentiated from each other by the “cisoide” rotameric configuration in turn to the carboxamide moiety [E_A (Figure 1D)]. These findings

Table 5. Chemical Shift Differences between Carboxamido (NH) Protons in ^1H NMR Spectra of 3-Hydroxy-2-pyrazinecarboxamides **1a–e** in Different Solvents at 25 °C

equivalent chemical shifts in ^1H -NMR

different chemical shifts in ^1H -NMR

1a–e (E_A) **1a'–e' (K_A)** X = F, Cl, Br, I, H

	$\Delta\delta$ (ppm) (range) ^a				
	H ₂ O	MeOH	MeCN	DMSO	CHCl ₃
1a	0.45 (8.48–8.03)	0.40 (8.36–7.96)	0.33 (7.76–7.43)	0.23 (8.73–8.50)	0.06 (8.00–7.94)
1b	0.94 (8.89–7.93)	0.49 (8.75–8.26)	0.21 (8.22–8.01)	0.26 (8.72–8.46)	0.05 (7.83–7.78)
1c	0.87 (8.26–7.39)	0.49 (8.75–8.26)	0.40 (8.12–7.72)	0.39 (8.58–8.19)	~0.00
1d	0.75 (8.94–8.19)	0.49 (7.51–7.02)	0.19 (8.56–8.37)	0.17 (8.56–8.39)	0.08 (7.74–7.66)
1e	1.37 (9.00–7.63)	0.82 (8.86–8.04)	0.71 (8.80–8.09)	0.63 (8.77–8.14)	0.62 (7.86–7.24)

^aChemical shift values were taken from the corresponding spectra in Figure 5.

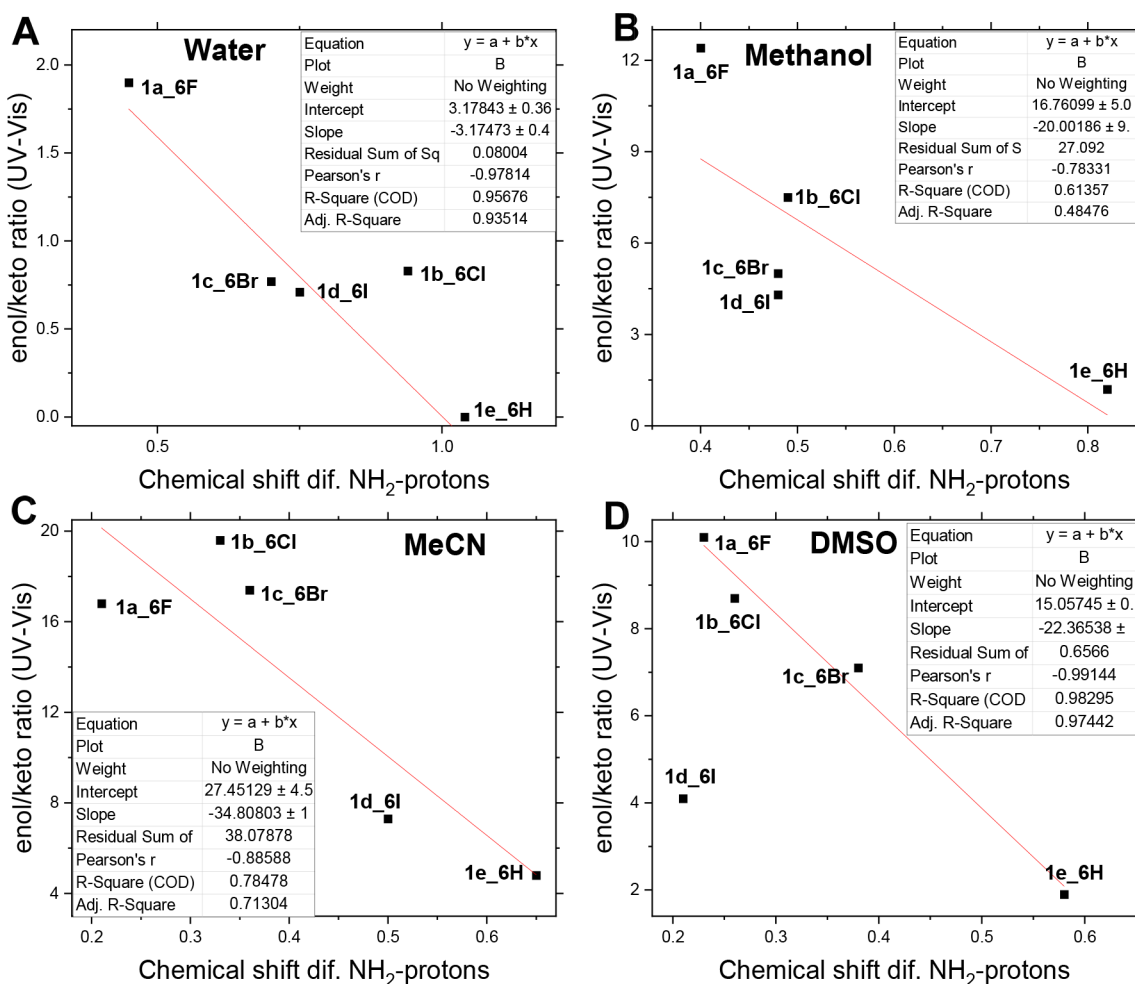


Figure 6. Correlation between the chemical shift (in parts per million) difference for carboxamido NH₂ protons from ^1H NMR with the keto:enol ratio from UV–vis measurements in (A) water, (B) methanol, (C) acetonitrile, and (D) DMSO.

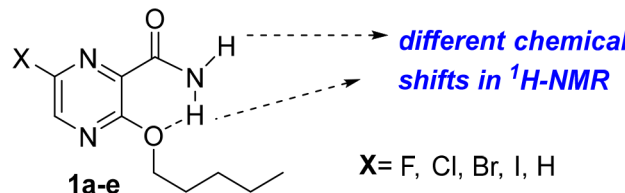
revealed that the rotamerism in 3-hydroxy-2-pyrazinecarboxamides **1a–e** is a chemical feature that is independent of aggregation state or external/internal electronic changes, being dependent on only the tautomerism of these molecules, where “cisoid” and “transoid” carboxamides are the preferred rotameric conformations for the enol and keto tautomers, respectively. Finally, Figure 6 shows that compound **1e** (6-H)

showed the largest chemical shift differences in any solvent (including chloroform; $\Delta\delta = 0.67$ ppm), whereas compound **1a** (6-F) showed the smallest chemical shift differences. Consequently, the keto and enol tautomers are the most preferred forms for compounds **1e** and **1a**, respectively, emerging as a starting point for rationally modulating the

tautomerism for the sake of convenience in this type of chemical system.

To obtain further information about the carboxamide rotamerism of this type of 3-hydroxypyrazine, we analyzed the rotamerism of 3-O-pentyl derivatives **2a–e** in solution from ^1H NMR measurements using solvents with varied polarity, i.e., methanol, acetone, and chloroform (Table 6).

Table 6. Chemical Shift Differences between Carboxamido NH_2 Protons in ^1H -NMR Spectra for 3-O-(Pentylloxy)-2-pyrazinecarboxamides **2a–e in Different Solvents at 25 °C**



1a–e **X = F, Cl, Br, I, H**

	$\Delta\delta$ (ppm) (range)		
	MeOH	acetone	CHCl_3
2a	0.34 (7.41–7.07)	0.56 (7.39–6.83)	1.16 (7.54–6.38)
2b	0.38 (6.66–6.28)	0.60 (7.55–6.95)	1.31 (7.46–6.15)
2c	0.32 (8.08–7.74)	0.59 (7.55–6.96)	1.33 (7.44–6.11)
2d	no NH_2 signal found	0.65 (7.41–6.76)	1.37 (7.34–5.97)
2e	0.39 (7.91–6.52)	0.71 (7.39–6.68)	1.36 (7.62–6.26)

From the results, appreciable chemical shift differences were observed between the carboxamide NH_2 protons and were dependent on the polarity and hydrogen bond nature of the solvent. Contrary to those of 3-hydroxy-2-pyrazinecarboxamides **1a–e**, the chemical shift differences increased with a decrease in the polarity solvents: chloroform > acetone > methanol. This suggests that the 3-O-alkylated analogues present a “transoide” conformation with an intramolecular hydrogen bond between the 3-oxygen and one of the carboxamido NH_2 protons (R–O–H–NHC=O) in an apolar solvent, whereas in a protic solvent, the “cisoide” rotameric conformation seems to be prevalent as determined by the small chemical shift difference. The results suggest that the “transoide” conformation is the most stable rotameric conformation of 3-O-alkylated derivatives **2a–e** because the intramolecular hydrogen bonding provides a major stabilization in the chemical system and the presence of a hydrogen-donor solvent probably compromises that stabilization by the preference of the 3-alkylated oxygen to interact via hydrogen bonding with the solvent. This latter facet induces the rotation of the carboxamide moiety toward the “cisoide” conformation in a protic solution to minimize the steric hindrance between the 3-oxo moiety and the 2-carboxamide. Thus, the rotamerism in 3-O-alkylated derivatives **2a–e** can be modulated by changes in solvent polarity. On the contrary, in the 3-hydroxy-2-pyrazinecarboxamide, the rotamerism is more dependent on the influence of the solvent because the presence of a 3-hydroxylic proton promoted the “cisoide” conformation by the extra stabilization via intramolecular hydrogen ($-\text{O–H–O=C–NH}_2$) bonding. Furthermore, it is important to mention that the interacting dynamic of the enol tautomer of the 3-hydroxy-2-pyrazinecarboxamides in a protic environment can involve another chemical phenomenon like a proton-transfer process to form the keto tautomer. Finally, like that of 3-hydroxy-2-pyrazinecarboxamides, the rotamerism of the 3-O-alkylated derivatives does not seem to depend on the

internal electronic changes because discrete changes in the chemical shift difference between the carboxamide protons are appreciated when a comparison is established for a common solvent, i.e., DMSO in Figures 5F. Further cases are illustrated in Figures S20–26.

Finally, we studied the effect of temperature on the equilibrium. The experiments were performed in $\text{DMSO-}d_6$ and a deuterated water environment for all five derivatives (**1a–e**) at 298, 313, and 328 K (Table S52). In that table, no appreciable changes were found for the chemical shift differences between the carboxamide NH_2 protons at the studied temperatures. The latter finding in conjunction with the similar enol:keto ratios found for the solid state and nonpolar solution suggests that the tautomerism of these 3-hydroxy-2-pyrazinecarboxamides is mainly governed by internal or external electronic changes. These internal and external electronic features were modulated by introduction of a specific substitution (F, Cl, Br, I, or H) with varied electronegativity at position 6 and by changes in the polarity of the solvent, respectively. In general, the proportion of the keto tautomer in solution was significantly increased with the polarity of the solvent for all studied derivatives **1a–e** as follows: water > methanol > ethanol > isopropanol > acetonitrile > DMSO > *n*-hexane. The strong preference of the keto tautomer in a protic solvent suggests that the tautomerization from the enol to keto form could be favored with an increase in the acidic or hydrogen-donor character of the solvent: water > methanol > ethanol > isopropanol. With regard to the internal electronic influence, the proportion of the keto tautomer consistently increased with a decrease in the electronegativity of the 6-substituent either for the solid state or for the solution state: $\text{H} \gg \text{I} > \text{Br} > \text{Cl} > \text{F}$ (Figure 7). The convergence of these two pieces of evidence reveals that the tautomerization from the enol to keto form in solution is facilitated by the hydrogen-donor character of the solvent and the basicity of pyrazine N4 (Figure 8). Calculation of the Mulliken charges on pyrazine N4 of the enolic 3-hydroxy-2-pyrazinecarboxamides **1a–e** showed that the basicity (reflected by high negative Mulliken charge values) was increased in the following order as a function of the electronegativity of the 6-substitution: $6\text{-H} > 6\text{-I} \sim 6\text{-Br} > 6\text{-Cl} \sim 6\text{-F}$. This allowed us to interpret the tautomerization in the studied 3-hydroxy-2-pyrazinecarboxamides as a function of the hydrogen-donor character of solvent and the basicity of pyrazine N4 as depicted in Figure 8.

3. CONCLUSIONS

In summary, this report offers a detailed perspective on the tautomerism and rotamerism in the gas, solid, and solution state for a series of 3-hydroxy-2-pyrazinecarboxamides. In general, we found that the tautomerism of the 3-hydroxy-2-pyrazinecarboxamides was dependent on internal or external electronic changes, it being possible to modulate the prevalence of a specific tautomer by altering the electronic nature of the 6-substitution (internal variable) and solvent polarity (external variable). Then, the keto tautomer was favored either in the solid state or in the solution state as a function of the 6-substitution: $\text{H} > \text{Br} > \text{I} > \text{Cl} \geq \text{F}$. The specificity in the tautomeric form was more controlled by solvent polarity, achieving almost 100% keto tautomer in water solution for some derivatives (**1c** and **1d** and strongly **1e**) and almost 100% enol tautomer in a nonpolar solvent for some derivatives (**1a** and **1b**). Then, the prevalence of the keto

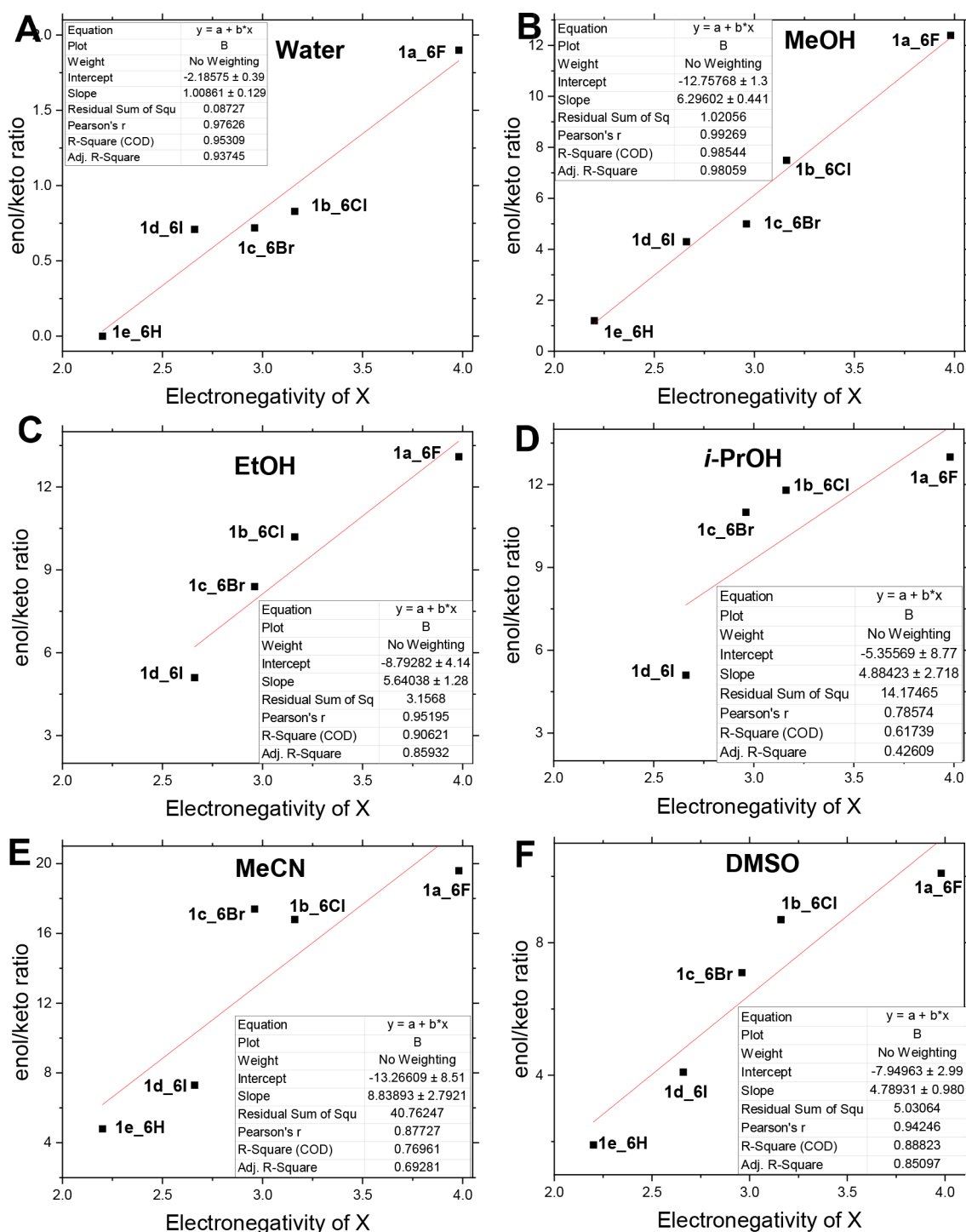


Figure 7. Correlation between the keto:enol ratio and the electronegativity of the substituent at position 6 in different environments: (A) water, (B) methanol, (C) ethanol, (D) isopropanol, (E) acetonitrile, and (F) DMSO.

tautomer was favored as a function of solvent polarity as follows: water > methanol > ethanol > isopropanol > CH₃CN > DMSO > *n*-hexane. All of these results allowed us to gain a better understanding on the factors governing the keto–enol equilibrium of 3-hydroxy-2-pyrazinecarboxamides, which could be of great interest for further study directed to control the antiviral activity of 3-hydroxy-2-pyrazinecarboxamides through control of the keto–enol equilibrium toward the keto form. In reference to the different proportions of antiviral ribonucleotides observed biologically for favipiravir and its dehalogenated

derivative (T-1105), our results are in complete agreement with these experimental data. The predominant tautomer, under all of the conditions, for T-1105 is the one that reacts with the anomeric carbon of furanose. The dependence of the tautomerism on the internal electronic features also presents a new possibility for modulating the occurrence of the keto tautomer, which could be preferred for a convenient drug metabolization to form the corresponding RTP metabolite. That tautomer can be favored with an increase in the basicity of tautomeric pyrazine N4, which can be modulated by

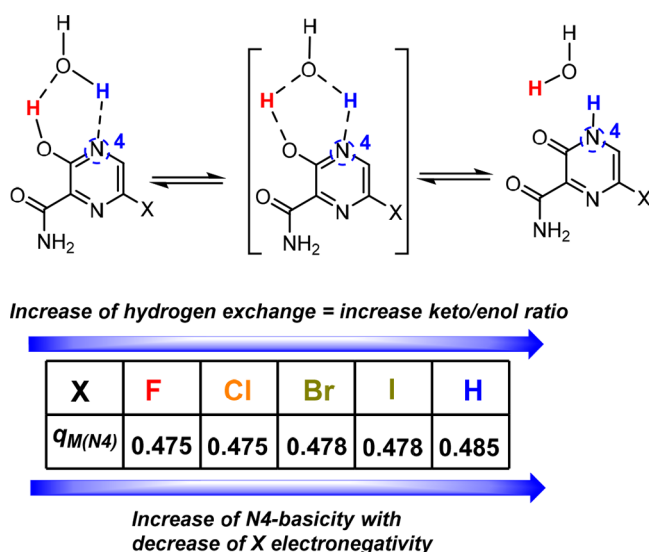


Figure 8. Tentative mechanism for tautomerization of the 3-hydroxy-2-pyrazinecarboxamides from the enol to keto tautomer as a function of internal (electronegativity of X) and external (protic solvent) electronic features. q_M is the Mulliken charge (expressed in arbitrary units) on pyrazine N4. Mulliken charge distributions were calculated at the B3LYP/6-31G(d,p) level for the enolic 3-hydroxy-2-pyrazinecarboxamides. A detailed Mulliken charge distribution can be found in Figure S44.

incorporation of a non-electron-deficient substituent at position 6 and including position 5 of the pyrazine core.

Moreover, we demonstrated that the rotamerism in turn in the 2-carboxamide was a function of the tautomerism, giving a “cisoide” rotameric configuration for the enol tautomer and a “transoide” rotameric form for the keto tautomer either in the solid state or in the solution state. This concept could play a role in the selective activity of this type of system as an RNA inhibitor, and its exact elucidation from a structural point of view is of great relevance for further interpretations. Also, from the point of view of organic synthesis, the elucidation of the tautomerism and rotamerism of these types of pyrazines is an important issue for understanding the factors that govern the direct fluorination of 3-hydroxy-2-pyrazinecarboxamide **1e** using Selectfluor.⁶³

4. EXPERIMENTAL SECTION

Materials and Instruments. 6-Fluoro-3-hydroxy-2-pyrazinecarboxamide (favipiravir) (**1a**) and 6-chloro-3-hydroxy-2-pyrazinecarboxamide (**1b**) were purchased from commercial sources (Jacky Zhou (Dideu)). The rest of the studied derivatives were synthesized from specific protocols. Details can be found in the synthetic procedures. Solvents (MeOH, isopropanol, MeCN, DMSO, CH₃COOH, and *n*-hexane) were anhydrous HPLC grade and purchased from commercial sources (Sigma-Aldrich, Fluka, or Merck). Ethanol was purchased from Droguera Industrial Uruguaya as a rectified ethanol (95%). Ultrapure grade water was obtained by filtration of deionized water with a Millipore system. Melting points are recorded with a micro melting point apparatus and are uncorrected. TLC was performed using commercially available 100–400 mesh silica gel plates (GF254), visualized under UV light (at 254 nm). Absorption data were obtained from a Thermo Scientific Varioskan Flash Multimode instrument for air-equilibrated solutions at 25 °C. ¹H NMR and ¹³C NMR spectra were recorded on a 400 MHz NMR spectrometer (Bruker-400). Multiplicity is indicated as follows: s, singlet; d, doublet; t, triplet; m, multiplet; dd, doublet of doublets; brs, broad singlet. Chemical shifts were measured in parts per million (δ),

and coupling constant (*J*) are given in hertz. Proton chemical shifts were given relative to tetramethylsilane (δ 0.00) in a CDCl₃ or DMSO-*d*₆ solvent. Carbon chemical shifts are internally referenced to the deuterated solvent signals in CDCl₃ (δ 77.00) or DMSO-*d*₆ (δ 40.02). IR spectroscopic analysis was performed on a Shimadzu IR Prestige 21 instrument. Single-crystal samples of these compounds were mounted on a glass tip, and data were collected in an Oxford Xcalibur Gemini Eos CCD diffractometer employing graphite-monochromated Mo Kα (λ = 0.71073 Å) radiation.

Synthesis of 3-Hydroxy-2-pyrazinecarboxamides 1c–e. 6-Bromo-3-hydroxy-2-pyrazinecarboxamide (**1c**),⁴⁸ 3-hydroxy-6-iodo-2-pyrazinecarboxamide (**1d**),⁴⁹ and 3-hydroxy-2-pyrazinecarboxamide (**1e**)⁴⁷ were prepared using reported protocols with a few modifications. Reaction mixtures were heated by using a sand bath. NMR spectra for compounds **1a–e** can be found in Figures S43–S65.

6-Fluoro-3-hydroxy-2-pyrazinecarboxamide (1a). R_f = 0.7 (AcOEt). Mp: 187–189 °C dec. ¹H NMR (400 MHz, DMSO-*d*₆): δ 13.52 (s, 1H), 8.70 (s, 1H), 8.54 (s, 1H), 8.46 (s, 1H). ¹³C{¹H} NMR (100 MHz, DMSO-*d*₆): δ 169.2, 160.2, 154.1–151.7 (*J* = 242.0 Hz, 1C), 136.2–135.9 (*J* = 35.0 Hz, 1C), 122.7 (*J* = 7.0 Hz, 1C). ¹⁹F NMR (500 MHz, CDCl₃): δ –92.73.

6-Chloro-3-hydroxy-2-pyrazinecarboxamide (1b). R_f = 0.6 (AcOEt). Mp: 199–201 °C dec. ¹H NMR (400 MHz, DMSO-*d*₆): δ 13.54 (s, 1H), 8.73 (s, 1H), 8.50 (s, 1H), 8.47 (s, 1H).

6-Bromo-3-hydroxy-2-pyrazinecarboxamide (1c). R_f = 0.5 (AcOEt). Mp: 238 °C dec. ¹H NMR (400 MHz, DMSO-*d*₆): δ 13.52 (s, 1H), 8.70 (s, 1H), 8.54 (s, 1H), 8.46 (s, 1H). ¹³C{¹H} NMR (100 MHz, DMSO-*d*₆): δ 168.55, 160.64, 148.10, 130.36 (CH), 126.30.

3-Hydroxy-6-iodo-2-pyrazinecarboxamide (1d). R_f = 0.5 (AcOEt). Mp: 207–209 °C dec. ¹H NMR (400 MHz, DMSO-*d*₆): δ 13.41 (s, 1H), 8.62 (s, 1H), 8.56 (s, 1H), 8.40 (s, 1H). ¹³C{¹H} NMR (100 MHz, DMSO-*d*₆): δ 179.89, 167.81, 161.85, 152.10, 134.38.

3-Hydroxy-2-pyrazinecarboxamide (1e). R_f = 0.2 (AcOEt). Mp: 247–250 °C dec (Lit. 251–253 °C). ¹H NMR (400 MHz, DMSO-*d*₆): δ 13.36 (s, 1H), 8.71 (s, 1H), 7.80–8.30 (m, 3H). ¹³C{¹H} NMR (100 MHz, DMSO-*d*₆): δ 167.36, 159.68, 140.10 (CH), 130.24 (CH), 122.02.

Typical Procedure for the O-Alkylation of the Halogenated 3-Hydroxypyrazine-2-carboxamides with *n*-Pentyl Iodide.⁵⁰ To a 10 mL bottom glass were added the corresponding 3-hydroxy-2-pyrazinecarboxamides **1a–e** (40 mg, 0.15–0.30 mmol, 1.0 equiv) and *n*-pentyl iodide (250–500 μL, 1.5–3.0 mmol, 10 equiv) under air. The mixture was stirred and heated at 100 °C for 12 h. The reaction mixture was monitored by TLC. The reaction mixture was purified by flash column chromatography using *n*-hexane/EtOAc (8:2) as the eluent to afford the product from fluorinated (**1a**), chlorinated (**1b**), and brominated (**1c**) derivativea, *n*-hexane/EtOAc (9:1) as the eluent to afford the iodated (**1d**) derivative, and *n*-hexane/EtOAc (6:4) as the eluent to afford the nonhalogenated compound (**1e**). The compounds were isolated as white solids. Reaction mixtures were heated using a sand bath. NMR spectra for compounds **2a–e** can be found in Figures S66–S102.

6-Fluoro-3-(pentylloxy)-2-pyrazinecarboxamide (2a). White solid (19.8 mg, 34%). Mp: 69–70 °C. ¹H NMR (400 MHz, CDCl₃): δ 8.15–8.13 (d, *J* = 8.0 Hz, 1H), 7.51 (br, 1H), 6.18 (br, 1H), 4.51 (t, 2H), 1.88 (m, 2H), 1.42 (m, 4H), 0.92 (t, 3H). ¹³C{¹H} NMR (100 MHz, CDCl₃): δ 163.3, 156.6, 155.10–152.78 (*J* = 232.0 Hz, 1C), 132.1–131.7 (*J* = 40.0 Hz, 1C), 128.3–128.2 (*J* = 7.0 Hz, 1C), 66.8, 28.4, 28.1, 22.4, 13.96. ¹⁹F NMR (500 MHz, CDCl₃): δ 92.27. Anal. Calcd for C₁₀H₁₄FN₂O₂: C, 52.86; H, 6.21; N, 18.49. Found: C, 52.72; H, 6.11; N, 18.40.

6-Chloro-3-(pentylloxy)-2-pyrazinecarboxamide (2b). White solid (17.4 mg, 31%). Mp: 74–76 °C. ¹H NMR (400 MHz, CDCl₃): δ 8.27 (s, 1H), 7.47 (br, 1H), 6.15 (br, 1H), 4.51 (t, 2H), 1.88 (m, 2H), 1.42 (m, 4H), 0.92 (t, 3H). ¹³C{¹H} NMR (100 MHz, CDCl₃): δ 163.5, 157.9, 143.8, 138.8, 132.0, 68.6, 28.3, 28.0, 22.4, 13.96. Anal. Calcd for C₁₀H₁₄ClN₂O₂: C, 49.29; H, 5.79; N, 17.24. Found: C, 49.21; H, 5.72; N, 17.20.

771 **6-Bromo-3-(pentyloxy)-2-pyrazinecarboxamide (2c)** (3.26 O-
772 substituted/N-substituted mixture). White solid (16.5 mg, 31%).
773 Mp: 95–97 °C. O-Substituted. ^1H NMR (400 MHz, CDCl_3): δ 8.35
774 (s, 1H), 7.44 (br, 1H), 6.13 (br, 1H), 4.51 (t, 2H), 1.88 (m, 2H), 1.42
775 (m, 4H), 0.92 (t, 3H). $^{13}\text{C}\{^1\text{H}\}$ NMR (100 MHz, CDCl_3): δ 161.5,
776 156.3, 144.6, 131.1, 126.4, 66.47, 26.3, 26.0, 20.3, 11.9. N-Substituted.
777 ^1H NMR (400 MHz, CDCl_3): δ 8.27 (s, 1H), 7.44 (br, 1H), 6.13 (br,
778 1H), 4.48 (t, 2H), 1.88 (m, 2H), 1.42 (m, 4H), 0.88 (t, 3H). $^{13}\text{C}\{^1\text{H}\}$
779 NMR (100 MHz, CDCl_3): δ 161.5, 155.8, 141.7, 136.7, 129.98, 66.5,
780 27.0, 26.3, 20.7, 12.1. Anal. Calcd for $\text{C}_{10}\text{H}_{14}\text{BrN}_3\text{O}_2$: C, 41.68; H,
781 4.90; N, 14.58. Found: C, 41.62; H, 4.85; N, 14.47.

782 **6-Iodo-3-(pentyloxy)-2-pyrazinecarboxamide (2d)**. White solid
783 (16.1 mg, 32%). Mp: 104–105 °C. ^1H NMR (400 MHz, CDCl_3): δ
784 8.43 (s, 1H), 7.35 (br, 1H), 5.98 (br, 1H), 4.51 (t, 2H), 1.88 (m, 2H),
785 1.42 (m, 4H), 0.92 (t, 3H). $^{13}\text{C}\{^1\text{H}\}$ NMR (100 MHz, CDCl_3): δ
786 162.7, 157.9, 151.1, 133.9, 101.2, 67.3, 27.3, 27.0, 21.3, 12.9. Anal.
787 Calcd for $\text{C}_{10}\text{H}_{14}\text{IN}_3\text{O}_2$: C, 35.84; H, 4.21; N, 12.54. Found: C, 35.76;
788 H, 4.17; N, 12.40.

789 **3-(Pentyloxy)-2-pyrazinecarboxamide (2e)**. White solid (23.5 mg,
790 39%). Mp: 93–94 °C. ^1H NMR (400 MHz, CDCl_3): δ 8.28 (s, 1H),
791 7.62 (br, 1H), 6.27 (br, 1H), 4.51 (t, 2H), 1.88 (m, 2H), 1.42 (m,
792 4H), 0.92 (t, 3H). $^{13}\text{C}\{^1\text{H}\}$ NMR (100 MHz, CDCl_3): δ 164.8, 158.9,
793 143.96, 136.1, 133.6, 67.7, 28.4, 28.1, 22.4, 13.97. Anal. Calcd for
794 $\text{C}_{10}\text{H}_{15}\text{N}_3\text{O}_2$: C, 57.40; H, 7.23; N, 20.08. Found: C, 57.31; H, 7.17;
795 N, 19.89.

796 **UV–Vis Spectroscopic Studies**. The UV–vis absorption spectra
797 were recorded for air-equilibrated solutions at room temperature.
798 Measurements were performed in a 96-well polystyrene plate
799 (NUNC). The UV–vis absorption spectra were recorded with a
800 UV–vis spectrophotometer at 2 nm resolution. A sample stock
801 DMSO solution (3 mM) was prepared, and the absorption spectra
802 were separately recorded with a 100 μL solution of water, EtOH,
803 MeOH, MeCN, DMSO, and *n*-hexane with 3.5% DMSO. All
804 absorption experiments were performed by triplicate. Absorption
805 spectra for derivatives 2a–e can be found in Figure S14.

806 **NMR Studies**. The ^1H NMR spectra of 3-hydroxy-2-pyrazine-
807 carboxamides 1a–e and O-alkylated derivatives 2a–e were recorded
808 under various conditions. A sample stock solution (D_2O , CD_3OD ,
809 MeCN, DMSO- d_6 , and CDCl_3) (10 mg in 0.5 mL) was prepared. ^{19}F
810 NMR spectra were recorded for derivatives 1a and 2a. Effects of
811 temperature at 298, 318, and 328 K were explored for some samples.
812 The time effect was measured at 0, 72, and 144 h. All experiments
813 were performed in triplicate. NMR spectra for tautomerism and
814 rotamerism with different environments, temperatures, and times can
815 be found in Figures S15–S42, and the effect of temperature is
816 presented in Table S53.

817 **Fourier Transformed Infrared (FTIR) Spectroscopy**. Solid
818 state IR spectra were directly recorded on a Bomen FTIR
819 spectrophotometer. IR spectra can be found in Figures S9–S13,
820 and IR spectroscopic data in Table S52.

821 **X-ray Data Collection and Structural Determination**. Light
822 white and yellow block-shaped crystals of compounds 1a–e and 2b–
823 d were obtained after slow evaporation of methanol, acetonitrile, and
824 chloroform solutions for 10 days. X-ray diffraction intensities were
825 collected (ω scans with θ and κ offsets), integrated, and scaled with
826 the CrysAlisPro26 suite of programs.⁵⁹ The unit cell parameters were
827 obtained by least-squares refinement (based on the angular settings
828 for all collected reflections with intensities larger than 7 times the
829 standard deviation of measurement errors) using CrysAlisPro. Data
830 were corrected empirically for absorption employing the multiscan
831 method implemented in CrysAlisPro. The structures were determined
832 by the intrinsic phasing procedure implemented in SHELXT,⁶⁰ and
833 the corresponding non-H molecular model was refined by a full-
834 matrix least-squares method on F^2 with anisotropic displacement
835 parameters employing SHELXL.⁶¹ Crystallographic structural data for
836 the eight structures have been deposited at the Cambridge
837 Crystallographic Data Centre (CCDC) with reference numbers
838 2240718 (1a), 2247867 (1b), 2240721 (1c), 2240760 (1d), 2247868
839 (1e), 2240766 (2b), 2247869 (2c), and 2247870 (2d). Details of the
840 crystallographic experiment can be seen in Tables S1–S3. Structural

data for bond lengths, bond angles, torsion angles, and hydrogen bond
distances are summarized in Tables S4–S33 for derivatives 1a–e and
in Tables S34–S51 for derivatives 2b–d. Crystal packing rearrange-
ment can be found in Figures S1–S8 for compounds 1a–e and 2b–d,
respectively.

Theoretical Calculation. All DFT calculations were carried out at
the Copernico Cluster of the computational center at Science Faculty
(Universidad Central Venezuela). All theoretical calculations, in the
gas phase, were performed using density functional theory (DFT)
with the Gaussian 09 quantum chemistry software.⁶² To achieve a
balance between the computational cost and the accuracy of the
calculations, two combined DFT-based approaches were employed:
(i) the M06-2X functional⁵¹ in combination with the def2TZVP basis
set⁵² and (ii) the B3LYP functional⁵³ in combination with the 6-
31G(d,p) basis set.⁵⁴ The geometries of the enol (1a–e) and keto
(1a'–e') tautomers of the 3-hydroxy-2-pyrazinecarboxamides were
optimized. Calculations were performed in the gas phase. All
structures were optimized in the ground state without restrictions,
using tight optimization criteria and an ultrafine grid in the
computation of two-electron integrals and their derivatives.
Optimization calculations were performed using the Berny algorithm
and were successfully completed with the following parameters:
maximum force, 0.000450; root-mean-square (RMS) force, 0.000300;
maximum displacement, 0.001800; RMS displacement, 0.001200;
predicted change in energy, -1.488276×10^{-8} Hartree for most
studied cases. The relative stability of the tautomers was presented as
the difference between the total energies of the enol and keto forms
($\Delta E = E_E - E_K$). A negative value indicates the more stable enol form
and vice versa. For conformational analysis, under the same B3LYP/6-
31G(d,p) approach, the calculations were performed using SCAN
commando with following parameters: RMS gradient normalization,
0.000311 hartree/Bohr; scan coordinate, 4.4567; maximum force,
0.000046; RMS force, 0.000014; maximum displacement, 0.001759;
RMS displacement, 0.000627; predicted energy change, -2.85×10^{-8}
hartree. Finally, for absorption wavelength calculations, the 10 lowest
excited states of compounds 1a–e were obtained from the optimized
structures at the time-dependent DFT (TD-DFT) level under
commando, td = (singlets, nstates = 10) using the B3LYP/6-31G(d,p)
approach.⁶⁴ The vibrational frequencies calculated numerically using
NUMFORCE showed that the excited state structures were minima
on the potential energy surface. The vibrational frequencies of the
stationary point geometries of the molecules (tautomers) were
calculated at the same computational level. Vibrational frequency
calculations were performed to obtain vibrational zero-point energies
and to validate that the located structures corresponded to the energy
minima. The structures should have only positive harmonic
vibrations. Theoretical UV–vis spectra for the enol and keto
tautomers of compounds 1a–e can be found in Figures S1 and S2
of the Theoretical Supporting Information (TSI). HOMO–LUMO
energy levels and Mulliken charges were extracted from optimized
geometries (Figures S3 and S4 of the TSI). All calculation outputs can
be found in the TSI.

■ ASSOCIATED CONTENT

Data Availability Statement

The data underlying this study are available in the published
article, in the Supporting Information, and openly in Mendeley
Data at DOI: 10.17632/tcrfh22jv5.1.

Supporting Information

The Supporting Information is available free of charge at
<https://pubs.acs.org/doi/10.1021/acs.joc.3c00777>.

UV–vis, IR, and NMR spectra in different environments
and detailed X-ray data (PDF)

Theoretical data (PDF)

Accession Codes

CCDC 2240718, 2240721, 2240760, 2240766, and 2247867–
2247870 contain the supplementary crystallographic data for 906

907 this paper. These data can be obtained free of charge via
908 www.ccdc.cam.ac.uk/data_request/cif, or by emailing data_request@ccdc.cam.ac.uk, or by contacting The Cambridge
909 Crystallographic Data Centre, 12 Union Road, Cambridge
910 CB2 1EZ, UK; fax: +44 1223 336033.

912 ■ AUTHOR INFORMATION

913 Corresponding Authors

914 **Angel H. Romero** – Grupo de Química Orgánica Medicinal,
915 Facultad de Ciencias, Universidad de la República, 11400
916 Montevideo, Uruguay; orcid.org/0000-0001-8747-5153;
917 Email: angel.ucv.usb@gmail.com

918 **Marcos Couto** – Grupo de Química Orgánica Medicinal,
919 Facultad de Ciencias, Universidad de la República, 11400
920 Montevideo, Uruguay; Email: mcouto@fcien.edu.uy

921 Authors

922 **Germán Fuentes** – Grupo de Química Orgánica Medicinal,
923 Facultad de Ciencias, Universidad de la República, 11400
924 Montevideo, Uruguay

925 **Leopoldo Suescun** – Cryssmat-Lab/DETEMA, Facultad de
926 Química, Universidad de la República, 11800 Montevideo,
927 Uruguay; orcid.org/0000-0002-7606-8074

928 **Oscar Piro** – Departamento de Física, Facultad de Ciencias
929 Exactas, Universidad Nacional de la Plata, La Plata 1900,
930 Argentina

931 **Gustavo Echeverría** – Departamento de Física, Facultad de
932 Ciencias Exactas, Universidad Nacional de la Plata, La Plata
933 1900, Argentina

934 **Lourdes Gotopo** – Laboratorio de Síntesis Orgánica, Escuela
935 de Química, Facultad de Ciencias, Universidad Central de
936 Venezuela, 1040 Caracas, Venezuela

937 **Horacio Pezaroglo** – Laboratorio de Resonancia Magnética
938 Nuclear, Facultad de Química, Universidad de la República,
939 11800 Montevideo, Uruguay

940 **Guzmán Álvarez** – Laboratorio de Moléculas Bioactivas,
941 CENUR Litoral Norte, Universidad de la República, 60000
942 Paysandú, Uruguay

943 **Gustavo Cabrera** – Laboratorio de Síntesis Orgánica, Escuela
944 de Química, Facultad de Ciencias, Universidad Central de
945 Venezuela, 1040 Caracas, Venezuela

946 **Hugo Cerecetto** – Grupo de Química Orgánica Medicinal,
947 Facultad de Ciencias, Universidad de la República, 11400
948 Montevideo, Uruguay; Area de Radiofarmacia, Centro de
949 Investigaciones Nucleares, Facultad de Ciencias, Universidad
950 de la República, 11400 Montevideo, Uruguay; orcid.org/0000-0003-1256-3786

952 Complete contact information is available at:
953 <https://pubs.acs.org/10.1021/acs.joc.3c00777>

954 Notes

955 The authors declare no competing financial interest.

956 ■ ACKNOWLEDGMENTS

957 This work was supported by the Comisión Sectorial de
958 Investigación Científica (CSIC, Uruguay), Universidad de la
959 República under the Program “Conocimiento especializado
960 para enfrentar la emergencia planteada por el COVID 19 y sus
961 impactos”. A.H.R., L.S., G.Á., H.C., and M.C. thank
962 PEDECIBA-Química (Uruguay) and Sistema Nacional de
963 Investigadores (SNI, Uruguay) for financial support. A.H.R.
964 thanks Agencia Nacional de Investigación e Innovación (ANII)
965 for financial support under code PD_NAC_2018_1_150515.

The authors are also grateful to Copernico Cluster (Facultad
de Ciencias, Universidad Central de Venezuela) for supplying
computational resources. The authors also thank CONICET
(Grant PIP 0651) and UNLP (Grant 11/X857) of Argentina
for financial support. G.E. and O.P. are Research Fellows of
CONICET.

■ REFERENCES

- (1) Singh, V.; Fedeles, B. I.; Essigmann, J. M. Role of tautomerism in RNA biochemistry. *RNA* **2015**, *21*, 1–13.
- (2) Fedeles, B. I.; Li, D.; Singh, V. Structural Insights Into Tautomeric Dynamics in Nucleic Acids and in Antiviral Nucleoside Analogs. *Front. Mol. Biosci.* **2022**, *8*, 823253.
- (3) Shukla, M. K.; Leszczynski, J. Tautomerism in nucleic acid bases and base pairs: a brief overview. *WIREs Computational Molecular Science* **2013**, *3*, 637–649.
- (4) Slocombe, L.; Al-Khalili, J. S.; Sacchi, M. Quantum and classical effects in DNA point mutations: Watson-Crick tautomerism in AT and GC base pairs. *Phys. Chem. Chem. Phys.* **2021**, *23*, 4141–4150.
- (5) Nemeria, N. S.; Chakraborty, S.; Balakrishnan, A.; Jordan, F. Reaction Mechanisms of Thiamin Diphosphate Enzymes: Defining States of Ionization and Tautomerization of the Cofactor at Individual Steps. *FEBS J.* **2009**, *276*, 2432–2446.
- (6) Beak, P. Energies and Alkylations of Tautomeric Heterocyclic Compounds: Old Problems - New Answers. *Acc. Chem. Res.* **1977**, *10*, 186–192.
- (7) Hass, M. A. S.; Hansen, D. F.; Christensen, H. E. M.; Led, J. J.; Kay, L. E. Characterization of Conformational Exchange of the Histidine Side Chain: Protonation, Rotamerization, and Tautomerization of His61 in Plastocyanin from *Anabaena variabilis*. *J. Am. Chem. Soc.* **2008**, *130*, 8460–8470.
- (8) Vila, J. A.; Arnautova, Y. A.; Vorobjev, Y.; Scheraga, H. A. Assessing the Fractions of Tautomeric Forms of the Imidazole Ring of Histidine in Proteins as a Function of pH. *Proc. Natl. Acad. Sci. U. S. A.* **2011**, *108*, 5602–5607.
- (9) Goodman, M. F. Mutations Caught in the Act. *Nature* **1995**, *378*, 237–238.
- (10) Jang, Y. H.; Goddard, W. A.; Noyes, K. T.; Sowers, L. C.; Hwang, S.; Chung, D. S. First Principles Calculations of the Tautomers and pKa Values of 8-Oxoguanine: Implications for Mutagenicity and Repair. *Chem. Res. Toxicol.* **2002**, *15*, 1023–1035.
- (11) Wang, W.; Hellinga, H. W.; Beese, L. S. Structural Evidence for the Rare Tautomer Hypothesis of Spontaneous Mutagenesis. *Proc. Natl. Acad. Sci. U.S.A.* **2011**, *108*, 17644–17648.
- (12) Guasch, L.; Yapamudiyansel, W.; Peach, M. L.; Kelley, J. A.; Barchi, J. J., Jr; Nicklaus, M. C. Experimental and Chemoinformatics Study of Tautomerism in a Database of Commercially Available Screening Samples. *J. Chem. Inf. Model.* **2016**, *56*, 2149–2161.
- (13) Li, D.; Fedeles, B. I.; Singh, V.; Peng, C. S.; Silvestre, K. J.; Simi, A. K.; Simpson, J. H.; Tokmakoff, A.; Essigmann, J. M. Tautomerism provides a molecular explanation for the mutagenic properties of the anti-HIV nucleoside 5-aza-5,6-dihydro-2'-deoxycytidine. *Proc. Natl. Acad. Sci. U. S. A.* **2014**, *111*, No. E3252–E3259.
- (14) Ortega-Prieto, A. M.; Sheldon, J.; Grande-Pérez, A.; Tejero, H.; Gregori, J.; Quer, J.; Esteban, J. I.; Domingo, E.; Perales, C. Extinction of hepatitis C virus by ribavirin in hepatoma cells involves lethal mutagenesis. *PLoS One* **2013**, *8*, No. e71039.
- (15) Dietz, J.; Schelhorn, S. E.; Fitting, D.; Mihm, U.; Susser, S.; Welker, M. W.; Füller, C.; Däumer, M.; Teuber, G.; Wedemeyer, H.; Berg, T.; Lengauer, T.; Zeuzem, S.; Herrmann, E.; Sarrazin, C. Deep sequencing reveals mutagenic effects of ribavirin during monotherapy of hepatitis C virus genotype 1-infected patients. *J. Virol.* **2013**, *87*, 6172–6181.
- (16) Moreno, H.; Grande-Pérez, A.; Domingo, E.; Martín, V. Arenaviruses and lethal mutagenesis. Prospects for new ribavirin-based interventions. *Viruses* **2012**, *4*, 2786–2805.
- (17) Graci, J. D.; Cameron, C. E. Quasispecies, error catastrophe, and the antiviral activity of ribavirin. *Virology* **2002**, *298*, 175–180.

- (18) Crotty, S.; Maag, D.; Arnold, J. J.; Zhong, W.; Lau, J. Y.; Hong, Z.; Andino, R.; Cameron, C. E. The broad-spectrum antiviral ribonucleoside ribavirin is an RNA virus mutagen. *Nat. Med.* **2000**, *6*, 1375–1379.
- (19) Slocombe, L.; Al-Khalili, J. S.; Sacchi, M. Quantum and classical effects in DNA point mutations: Watson-Crick tautomerism in AT and GC base pairs. *Phys. Chem. Chem. Phys.* **2021**, *23*, 4141–4150.
- (20) Baranovich, T.; Wong, S. S.; Armstrong, J.; Marjuki, H.; Webby, R. J.; Webster, R. G.; Govorkova, E. A. T-705 (favipiravir) induces lethal mutagenesis in influenza A H1N1 viruses in vitro. *J. Virol.* **2013**, *87*, 3741–3751.
- (21) Domingo, E.; Martin, V.; Perales, C.; Grande-Pérez, A.; García-Arriaza, J.; Arias, A. Viruses as quasispecies: Biological implications. *Curr. Top. Microbiol. Immunol.* **2006**, *299*, 51–82.
- (22) Schäker-Hübner, L.; Haschemi, R.; Büch, T.; Kraft, F. B.; Brumme, B.; Schöler, A.; Jenke, R.; Meiler, J.; Aigner, A.; Bendas, G.; Hansen, F. K. Balancing Histone Deacetylase (HDAC) Inhibition and Drug-likeness: Biological and Physicochemical Evaluation of Class I Selective HDAC Inhibitors. *ChemMedChem* **2022**, *17*, No. e202100755.
- (23) Nicholls, A.; McGaughey, G. B.; Sheridan, R. P.; Good, A. C.; Warren, G.; Mathieu, M.; Muchmore, S. W.; Brown, S. P.; Grant, J. A.; Haigh, J. A.; Nevins, N.; Jain, A. N.; Kelley, B. Molecular Shape and Medicinal Chemistry: A Perspective. *J. Med. Chem.* **2010**, *53*, 3862–3886.
- (24) Furuta, Y.; Takahashi, K.; Fukuda, Y.; Kuno, M.; Kamiyama, T.; Kozaki, K.; Nomura, N.; Egawa, H.; Minami, S.; Watanabe, Y.; Narita, H.; Shiraki, K. In vitro and in vivo activities of anti-influenza virus compound T-705. *Antimicrob. Agents Chemother.* **2002**, *46*, 977–981.
- (25) Kiso, M.; Takahashi, K.; Sakai-Tagawa, Y.; Shinya, K.; Sakabe, S.; Le, Q. M.; Ozawa, M.; Furuta, Y.; Kawaoka, Y. T-705 (favipiravir) activity against lethal H5N1 influenza A viruses. *Proc. Natl. Acad. Sci. U.S.A.* **2010**, *107*, 882–887.
- (26) Gowen, B. B.; Wong, M. H.; Jung, K. H.; Smee, D. F.; Morrey, J. D.; Furuta, Y. Efficacy of favipiravir (T-705) and T-1106 pyrazine derivatives in phlebovirus disease models. *Antiviral Res.* **2010**, *86*, 121–127.
- (27) Morrey, J. D.; Taro, B. S.; Siddharthan, V.; Wang, H.; Smee, D. F.; Christensen, A. J.; Furuta, Y. Efficacy of orally administered T-705 pyrazine analog on lethal West Nile virus infection in rodents. *Antiviral Res.* **2008**, *80*, 377–379.
- (28) Rocha-Pereira, J.; Jochmans, D.; Dallmeier, K.; Leyssen, P.; Nascimento, M. S. J.; Neyts, J. Favipiravir (T-705) inhibits in vitro norovirus replication. *Biochem. Biophys. Res. Commun.* **2012**, *424*, 777–780.
- (29) Yamada, K.; Noguchi, K.; Komeno, T.; Furuta, Y.; Nishizono, A. Efficacy of favipiravir (T-705) in rabies postexposure prophylaxis. *J. Infect. Dis.* **2016**, *213*, 1253–1261.
- (30) Gowen, B. B.; Wong, M. H.; Jung, K. H.; Sanders, A. B.; Mendenhall, M.; Bailey, K. W.; Furuta, Y.; Sidwell, R. W. In vitro and in vivo activities of T-705 against arenavirus and bunyavirus infections. *Antimicrob. Agents Chemother.* **2007**, *51*, 3168–3176.
- (31) Oestereich, L.; Lüdtke, A.; Wurr, S.; Rieger, T.; Muñoz-Fontela, C.; Günther, S. Successful treatment of advanced Ebola virus infection with T-705 (favipiravir) in a small animal model. *Antiviral Res.* **2014**, *105*, 17–21.
- (32) Furuta, Y.; Komeno, T.; Nakamura, T. Favipiravir (T-705), A Broad Spectrum Inhibitor of Viral RNA Polymerase. *Proc. Jpn. Acad. Ser. B Phys. Biol. Sci.* **2017**, *93*, 449–463.
- (33) Manabe, T.; Kambayashi, D.; Akatsu, H.; Kudo, K. Favipiravir for the treatment of patients with COVID-19: a systematic review and meta-analysis. *BMC Infect. Dis.* **2021**, *21*, 489–501.
- (34) Lai, C. C.; Chao, C. M.; Hsueh, P. R. Clinical efficacy of antiviral agents against coronavirus disease 2019: A systematic review of randomized controlled trials. *J. Microbiol. Immunol. Infect.* **2021**, *54*, 767–775.
- (35) <https://clinicaltrials.gov>.
- (36) Joshi, S.; Parkar, J.; Ansari, A.; Vora, A.; Talwar, D.; Tiwaskar, M.; Patil, S.; Barkate, H. Role of favipiravir in the treatment of COVID-19. *Int. J. Infect. Dis.* **2021**, *102*, 501–508.
- (37) Joshi, S.; Vora, A.; Venugopal, K.; Dadhich, P.; Daxini, A.; Bhagat, S.; Patil, S.; Barkate, H. Real-World Experience with Favipiravir for the Treatment of Mild-to-Moderate COVID-19 in India. *Pragmatic Obs. Res.* **2022**, *13*, 33–41.
- (38) De Savi, C.; Hughes, D. L.; Kvaerno, L. Quest for a COVID-19 Cure by Repurposing Small-Molecule Drugs: Mechanism of Action, Clinical Development, Synthesis at Scale, and Outlook for Supply. *Org. Process Res. Dev.* **2020**, *24*, 940–976.
- (39) Al Bujug, N. Methods of Synthesis of Remdesivir, Favipiravir, Hydroxychloroquine, and Chloroquine: Four Small Molecules Repurposed for Clinical Trials during the Covid-19 Pandemic. *Synthesis* **2020**, *52*, 3735–3750.
- (40) Chakraborty, C.; Sharma, A. R.; Bhattacharya, M.; Agoramoorthy, G.; Lee, S. S. The Drug Repurposing for COVID-19 Clinical Trials Provide Very Effective Therapeutic Combinations: Lessons Learned From Major Clinical Studies. *Front. Pharmacol.* **2021**, *12*, 704205.
- (41) Gaonkar, S. L.; Deepika, D.; Hakkimane, S. S. Favipiravir (6-Fluoro-3-hydroxy-2-pyrazinecarboxamide) a Broad Spectrum Inhibitor of Viral RNA Polymerase in COVID-19 Treatment. *Chem. Select* **2021**, *6*, 12652–12662.
- (42) (a) Huchting, J.; Vanderlinden, E.; Van Berwaer, R.; Meier, C.; Naesens, L. Cell line-dependent activation and antiviral activity of T-1105, the non-fluorinated analogue of T-705 (favipiravir). *Antiviral Res.* **2019**, *167*, 1–5. (b) Furuta, Y.; Takahashi, K.; Shiraki, K.; Sakamoto, K.; Smee, D. F.; Barnard, D. L.; Gowen, B. B.; Julander, J. G.; Morrey, J. D. T-705 (favipiravir) and related compounds: Novel broad-spectrum inhibitors of RNA viral infections. *Antiviral Res.* **2009**, *82*, 95–102. (c) Huchting, J.; Vanderlinden, E.; Winkler, M.; Nasser, H.; Naesens, L.; Meier, C. Prodrugs of the Phosphoribosylated Forms of Hydroxypyrazinecarboxamide Pseudobase T-705 and Its De-Fluoro Analogue T-1105 as Potent Influenza Virus Inhibitors. *J. Med. Chem.* **2018**, *61*, 6193–6210.
- (43) (a) Assis, L. C.; Alves de Castro, A.; Almirao de Jesus, J. P.; Ferreira da Cunha, L. F.; Nepovimova, E.; Krejcar, O.; Kuca, K.; Castro Ramalho, T.; de Almeida La Porta, F. Theoretical insights into the effect of halogenated substituent on the electronic structure and spectroscopic properties of the favipiravir tautomeric forms and its implications for the treatment of COVID-19. *RSC Adv.* **2021**, *11*, 35228. (b) Du, Y. X.; Chen, X. P. Favipiravir: Pharmacokinetics and Concerns About Clinical Trials for 2019-nCoV Infection. *Clin. Pharm. Ther.* **2020**, *108*, 242–247.
- (44) (a) Deneva, V.; Slavova, S.; Kumanova, A.; Vassilev, N.; Nedeltcheva-Antonova, D.; Antonov, L. Favipiravir-tautomeric and complexation properties in solution. *Pharmaceuticals* **2023**, *16*, 45. (b) Antonov, L. Favipiravir tautomerism: a theoretical insight. *Theor. Chem. Acc.* **2020**, *139*, 145. (c) Konstantinova, I. D.; Andronova, V. L.; Fateev, I. V.; Esipov, R. S. Favipiravir and its structural analogs: Antiviral activity and synthesis methods. *Acta Naturae* **2022**, *14*, 16–38. (d) Babashkina, M. G.; Frontera, A.; Kertman, A. V.; Saygideger, Y.; Murugavel, S.; Safin, D. A. Favipiravir: insight into the crystal structure, Hirshfeld surface analysis and computational study. *J. Iranian Chem. Soc.* **2022**, *19*, 85–94. (e) Tiyasakulchai, T.; Charoensetukul, N.; Khamkhenshorgphanuch, T.; Thongpanchang, C.; Srikun, O.; Yuthavong, Y.; Srimongkolpithak, N. Scalable synthesis of favipiravir via conventional and continuous flow chemistry. *RSC Adv.* **2021**, *11*, 38691. (f) Umar, Y. Theoretical studies of the rotational and tautomeric states, electronic and spectroscopic properties of favipiravir and its structural analogues: a potential drug for the treatment of COVID-19. *J. Taibah Univ. Sci.* **2020**, *14*, 1613–1625. (g) Yasir, H. M.; Hanoon, F. H. DFT and TD-DFT Study of Favipiravir Tautomerism as RNA Polymerase Inhibitors: COVID-19. *IOP Conf. Ser.: Mater. Sci. Eng.* **2020**, *928*, 072066.
- (45) (a) Sato, N.; Matsumoto, K.; Takishima, M.; Mochizuki, K. Studies on pyrazines. Part 34.1 Synthetic approach, stability and tautomerism of 2,6-dihydroxypyrazines. *J. Chem. Soc. Perk. Trans. 1*

- 1169 **1997**, *21*, 3167–3172. (b) Cheeseman, G. W. H.; Godwin, R. A.
1170 Pyrazines. Part IV. 2,6-Dihydroxy-3,5-diphenylpyrazine and related
1171 compounds. *J. Chem. Soc. C* **1971**, 2977–2979. (c) Sato, N. In
1172 *Comprehensive Heterocyclic Chemistry*, 2nd ed.; Katritzky, A. R., Rees,
1173 C. W., Scriven, E. F. V., Eds.; Pergamon: Oxford, U.K., 1996; Vol. 6, p
1174 241.
- 1175 (46) (a) Hatherley, L. D.; Brown, R. D.; Godfrey, P. D.; Pierlot, A.
1176 P.; Caminati, W.; Damiani, D.; Melandri, S.; Favero, L. B. *J. Phys.*
1177 *Chem.* **1993**, *97*, 46. (b) Mata, S.; Cortijo, V.; Caminati, W.; Alonso, J.
1178 L.; Sanz, M. E.; Lopez, J. C.; Blanco, S. Tautomerism and
1179 Microsolvation in 2-Hydroxypyridine/2-Pyridone. *J. Phys. Chem. A*
1180 **2010**, *114*, 11393–11398.
- 1181 (47) Toyama Chemical Co. Ltd. Method for producing 3-hydroxy-2-
1182 pyrazinecarboxamide. JP 5739618 B2, 2015.
- 1183 (48) Method for producing 3,6-dichloro-2-pyrazinecarbonitrile. JP
1184 5559604B2.
- 1185 (49) Fused ring heterocycle kinase modulators. WO 2006/015124,
1186 2006.
- 1187 (50) Feng, B.; Li, Y.; Li, H.; Zhang, X.; Xie, H.; Cao, H.; Yu, L.; Xu,
1188 Q. Specific N-Alkylation of Hydroxypyridines Achieved by a Catalyst
1189 and Base-Free Reaction with Organohalides. *J. Org. Chem.* **2018**, *83*,
1190 6769–6775.
- 1191 (51) Zhao, Y.; Truhlar, D. G. The M06 suite of density functionals
1192 for main group thermochemistry, thermochemical kinetics, non-
1193 covalent interactions, excited states, and transition elements: two new
1194 functionals and systematic testing of four M06-class functionals and
1195 12 other functionals. *Theor. Chem. Acc.* **2008**, *120*, 215–241.
- 1196 (52) Weigend, F.; Ahlrichs, R. Balanced basis sets of split valence,
1197 triple zeta valence and quadruple zeta valence quality for H to Rn:
1198 design and assessment of accuracy. *Phys. Chem. Chem. Phys.* **2005**, *7*,
1199 3297.
- 1200 (53) Becke, A. D. A new mixing of Hartree-Fock and local density-
1201 functional theories. *J. Chem. Phys.* **1993**, *98*, 1372.
- 1202 (54) Petersson, G. A.; Al-Laham, M. A. A Complete Basis Set Model
1203 Chemistry. II. Open-Shell Systems and the Total Energies of the First-
1204 Row Atoms. *J. Chem. Phys.* **1991**, *94*, 6081–6090.
- 1205 (55) Romero, A. H.; Squitieri, E. Effect of heterosubstituent and ring
1206 puckering angle on linear and nonlinear properties of exo-insaturated
1207 four-membered heterocycles, $Y = CCH_2CH_2X$: A comparative ab
1208 initio, DFT and semi-empirical study. *Mol. Phys.* **2016**, *114*, 2232–
1209 2247.
- 1210 (56) Romero, A. H. A theoretical conformational study on the
1211 structural parameters involved in the ring strain of exo-insaturated
1212 four-membered heterocycles, $YCCH_2CH_2X$. *Mol. Phys.* **2016**, *114*,
1213 3040–3054.
- 1214 (57) Romero, A. H.; Squitieri, E. Potential use of small basis set on
1215 the calculations of electronic properties of some four-membered
1216 heterocycles: A conformational study. *Mol. Phys.* **2017**, *115*, 261–277.
- 1217 (58) Romero, A. H. A theoretical conformational study on the
1218 multipole moment of exo-insaturated four-membered heterocycles,
1219 $Y = CCH_2CH_2X$. *Mol. Phys.* **2017**, *115*, 2528–2546.
- 1220 (59) *CrysAlisPro*, ver. 1.171.38.41; Rigaku Oxford Diffraction, 2015.
- 1221 (60) Sheldrick, G. M. SHELXT-Integrated Space-Group and
1222 Crystal-Structure Determination. *Acta Crystallogr.* **2015**, *A71*, 3–8.
- 1223 (61) Sheldrick, G. M. A Short History of SHELX. *Acta Crystallogr.*
1224 **2008**, *A64*, 112–122.
- 1225 (62) Frisch, M. J.; Trucks, G. W.; Schlegel, H. B.; Scuseria, G. E.;
1226 Robb, M. A.; Cheeseman, J. R.; Scalmani, G.; Barone, V.; Mennucci,
1227 B.; Petersson, G. A.; et al. *Gaussian 09*, rev. A.1; Gaussian, Inc.:
1228 Wallingford, CT, 2009.
- 1229 (63) Fuentes, G.; García, M. F.; Cerecetto, H.; Álvarez, G.; Couto,
1230 M.; Romero, A. H. One-Step Synthesis of Favipiravir from
1231 Selectfluor® and 3-Hydroxy-2-pyrazinecarboxamide in Ionic Liquid.
1232 *Org. Biomol. Chem.* **2023**, *21*, 3660–3668.
- 1233 (64) Benkyi, I.; Tapavicza, E.; Fliegl, H.; Sundholm, D. Calculation
1234 of vibrationally resolved absorption spectra of acenes and pyrene.
1235 *Phys. Chem. Chem. Phys.* **2019**, *21*, 21094–21103.